DEVELOPMENT OF PROTOCOL TO MAINTAIN WINTER MOBILITY OF DIFFERENT CLASSES OF PERVIOUS CONCRETE PAVEMENT BASED ON POROSITY

FINAL PROJECT REPORT

by

Somayeh Nassiri, Assistant Professor
Othman Alsharedah, PhD Student
Washington State University

DISCLAIMER

The contents of this report reflect the views of the authors, who are responsible for the facts and the accuracy of the information presented herein. This document is disseminated under the sponsorship of the U.S. Department of Transportation's University Transportation Centers Program, in the interest of information exchange. The Pacific Northwest Transportation Consortium, the U.S. Government and matching sponsor assume no liability for the contents or use thereof.

Technical Report Documentation Page		
1. Report No.	**2. Government Accession No.** 01701503	**3. Recipient's Catalog No.**
4. Title and Subtitle Development of protocol to maintain winter mobility of different classes of pervious concrete pavement based on porosity	**5. Report Date** December 15, 2019	
	6. Performing Organization Code	
7. Author(s) and Affiliations Somayeh Nassiri, Assistant Professor, Washington State University ORCID# 0000-0001-5367-2167 Othman Alshareedah, Ph.D. Student, Washington State University	**8. Performing Organization Report No.** 2017-S-WSU-3	
9. Performing Organization Name and Address PacTrans Pacific Northwest Transportation Consortium University Transportation Center for Federal Region 10 University of Washington More Hall 112 Seattle, WA 98195-2700	**10. Work Unit No. (TRAIS)**	
	11. Contract or Grant No. 69A3551747110	
12. Sponsoring Organization Name and Address United States Department of Transportation Research and Innovative Technology Administration 1200 New Jersey Avenue, SE Washington, DC 20590	**13. Type of Report and Period Covered** Final report (09/01/2017-12/31/2019)	
	14. Sponsoring Agency Code	
15. Supplementary Notes Report uploaded to: www.pactrans.org		

16. Abstract

The main focus of this study was to develop an image-based method to characterize the porosity of in-situ pervious concrete (PC), so this feature can be correlated with ice formation and winter maintenance operations of the pavement. First, a surface imaging-based porosity characterization method was investigated. A total of 27 PC slabs cast at three targeted porosity levels—15 percent, 25 percent, and 35 percent--were used. Images of the top and bottom surfaces of the slabs were used in thresholding techniques, in which the images were binarized and the area of the voids were obtained. The image-based porosity was calculated as the ratio of the area of voids to the total surface area of each slab. The image-based porosity was correlated with the porosity of the PC measured in accordance with ASTM C1754 by submersion. For validation, the distribution of the porosity along the depth of PC cores extracted from the slabs was quantified from images taken by X-ray computed tomography (CT). Analysis of these images revealed that the distribution of pores along the depth were significantly different at intermediate depths than that at the top and bottom 0.5-inch depths because of compaction. Therefore, the developed surface image-based method did not provide a representative porosity value for the full PC layer. More surface imaging, in parallel with X-ray CT scans, are required to develop a correlation between the porosity of the surface layer and overall porosity. Finally, the Gibbs-Thompson equation, a thermodynamic-based model developed in past studies, was recommended to determine the critical temperature at which ice formation initiates inside PC pores. The proposed image-based porosity characterization method and the Gibbs-Thompson equation can be used as a decision support tool for transportation authorities to identify the time of ice formation in PC pavements in order to apply timely winter maintenance treatments.

17. Key Words Pervious concrete, porosity, X-ray, computed tomography, image analysis		**18. Distribution Statement**	
19. Security Classification (of this report) Unclassified.	**20. Security Classification (of this page)** Unclassified.	**21. No. of Pages** 25	**22. Price** N/A

Form DOT F 1700.7 (8-72)   **Reproduction of completed page authorized.**

SI* (Modern Metric) Conversion Factors

APPROXIMATE CONVERSIONS TO SI UNITS				
Symbol	When You Know	Multiply By	To Find	Symbol
LENGTH				
in	inches	25.4	millimeters	mm
ft	feet	0.305	meters	m
yd	yards	0.914	meters	m
mi	miles	1.61	kilometers	km
AREA				
in^2	square inches	645.2	square millimeters	mm^2
ft^2	square feet	0.093	square meters	m^2
yd^2	square yard	0.836	square meters	m^2
ac	acres	0.405	hectares	ha
mi^2	square miles	2.59	square kilometers	km^2
VOLUME				
fl oz	fluid ounces	29.57	milliliters	mL
gal	gallons	3.785	liters	L
ft^3	cubic feet	0.028	cubic meters	m^3
yd^3	cubic yards	0.765	cubic meters	m^3
	NOTE: volumes greater than 1000 L shall be shown in m^3			
MASS				
oz	ounces	28.35	grams	g
lb	pounds	0.454	kilograms	kg
T	short tons (2000 lb)	0.907	megagrams (or "metric ton")	Mg (or "t")
TEMPERATURE (exact degrees)				
°F	Fahrenheit	5 (F-32)/9 or (F-32)/1.8	Celsius	°C
ILLUMINATION				
fc	foot-candles	10.76	lux	lx
fl	foot-Lamberts	3.426	candela/m^2	cd/m^2
FORCE and PRESSURE or STRESS				
lbf	poundforce	4.45	newtons	N
lbf/in^2	poundforce per square inch	6.89	kilopascals	kPa

APPROXIMATE CONVERSIONS FROM SI UNITS				
Symbol	When You Know	Multiply By	To Find	Symbol
LENGTH				
mm	millimeters	0.039	inches	in
m	meters	3.28	feet	ft
m	meters	1.09	yards	yd
km	kilometers	0.621	miles	mi
AREA				
mm^2	square millimeters	0.0016	square inches	in^2
m^2	square meters	10.764	square feet	ft^2
m^2	square meters	1.195	square yards	yd^2
ha	hectares	2.47	acres	ac
km^2	square kilometers	0.386	square miles	mi^2
VOLUME				
mL	milliliters	0.034	fluid ounces	fl oz
L	liters	0.264	gallons	gal
m^3	cubic meters	35.314	cubic feet	ft^3
m^3	cubic meters	1.307	cubic yards	yd^3
MASS				
g	grams	0.035	ounces	oz
kg	kilograms	2.202	pounds	lb
Mg (or "t")	megagrams (or "metric ton")	1.103	short tons (2000 lb)	T
TEMPERATURE (exact degrees)				
°C	Celsius	1.8C+32	Fahrenheit	°F
ILLUMINATION				
lx	lux	0.0929	foot-candles	fc
cd/m^2	candela/m^2	0.2919	foot-Lamberts	fl
FORCE and PRESSURE or STRESS				
N	newtons	0.225	poundforce	lbf
kPa	kilopascals	0.145	poundforce per square inch	lbf/in^2

*SI is the symbol for the International System of Units. Appropriate rounding should be made to comply with Section 4 of ASTM E380.
(Revised March 2003)

Table of Contents

LIST OF FIGURES

LIST OF TABLES

Acknowledgments

Executive Summary

The increasing use of pervious concrete (PC) pavement (PCP) in the Pacific Northwest region (PNW) requiring effective winter maintenance operations to ensure the safety and mobility of drivers and pedestrians. To improve such effective practices, a porosity-based characterization method for PCP was proposed in this study so that the skid resistance of PC with various porosity and ice formation patterns in the pores can be characterized in the future. In a previous PacTrans project, 27 PC slabs were cast with three targeted porosity levels—15 percent, 25 percent, and 35 percent. Then, using an eight-megapixel, consumer-grade digital camera, the slabs' surfaces were photographed and reviewed with an image processing technique (figure. A). This method quantified the porosity as the ratio of voids area to the total surface area of the slab. The proposed image-based method provides an easy method to characterize the clogging and ice formation of PCP by using ubiquitous cell phone or digital cameras.
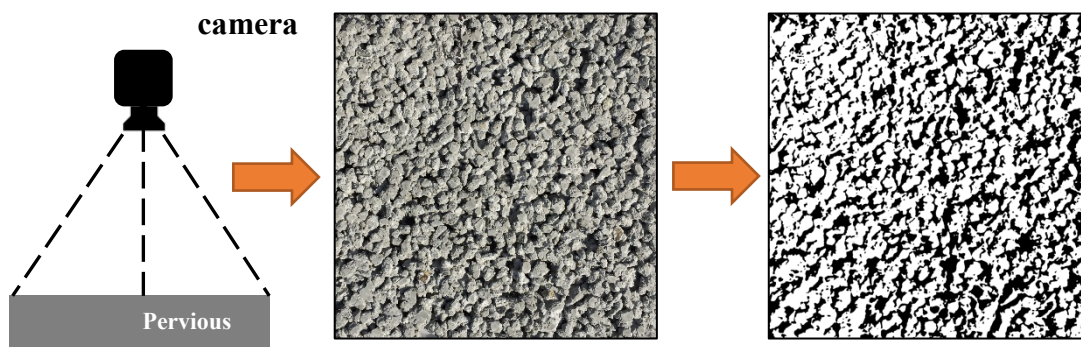
Figure A. Image binarization to obtain the area of voids (black areas in the binarized image)

A regression model was developed to correlate image-based porosity with the porosity measured according to ASTM C1754 with the submersion method. The latter method is commonly used on core specimens. Use of the submersion method, however, would require

destructive coring of the pavement. Therefore, a correlation between the results of the submersion method and the image-based method developed in this study could eliminate the need for coring. Note that PC from one mixture design made with angular-shaped aggregates in a specific particle size distribution was used to develop the image-based porosity method. Testing of mixtures with aggregates of other shapes and other mix designs would expand the database and increase the application of the developed method. Once expanded, the method could be used in an application software so that users could instantly quantify the conditions of the pavement surface by using their cell phone camera.

For validation, a representative slab from each porosity level was cored, and the cores were used for X-ray computed tomography (X-ray CT) analysis. For each core, around 1600 two-dimensional images (2D slices) of the cores' cross-section along the vertical direction were acquired with X-ray CT. From the 2D slices, the exact porosity and porosity distribution along the depth of each slab were obtained. The porosity results from the X-ray CT analysis and the submersion porosity (ASTM C1754) were in good agreement. The results of the porosity distribution along the depth of the slabs indicated that for low-porosity specimens, the variation of porosity along the depth was lower than that of the specimens with high porosity (see figure B). This was due to the high compaction applied to the fresh PC during casting of the low-porosity specimens. In contrast, specimens with high targeted porosity received less compaction, which resulted in high porosity at the surface and lower porosity at the mid-depth region. The X-ray CT results confirmed that image-based porosity was always higher than the overall porosity (measured on the basis of ASTM C1754).
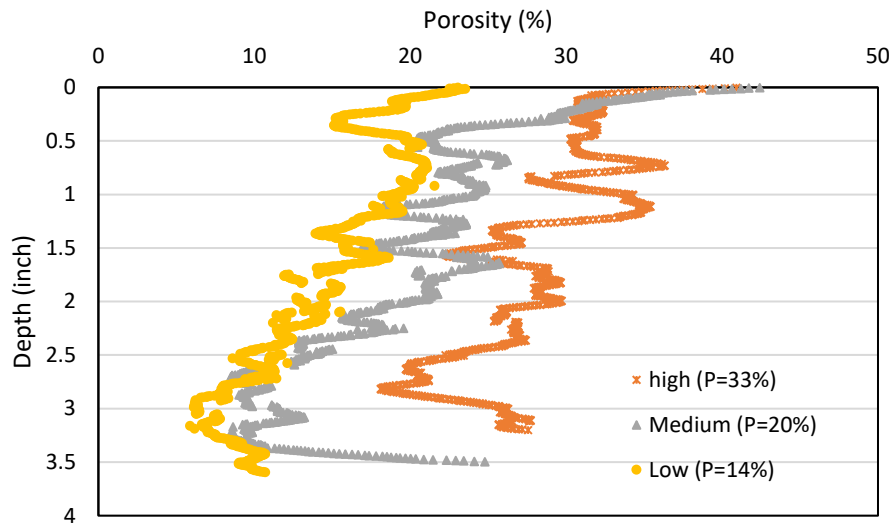
Figure B. Porosity distribution along the depth of the cores

The effect of porosity on the infiltration rate of PCP was investigated, and a correlation between porosity and infiltration rate was established. Moreover, field test results of the skid resistance of PCP using the British Pendulum Tester (BPT) did not show a statistically significant correlation with porosity. Further research is needed to identify other tests that can be used to quantify the in-situ skid resistance of PCP to reflect the effect of the pores. In addition, a theoretical model developed in past studies was proposed to determine the critical temperature at which ice will form in PCP and when maintenance such as the application of deicers is needed. This model, along with the image-based porosity method, can serve as a decision support tool for PCP maintenance during winter conditions.

CHAPTER 1. Introduction

1.1. <u>Winter Maintenance of Permeable Pavements</u>

Pervious concrete (PC) pavement (PCP) is increasingly used by the municipalities in the Pacific Northwest (PNW) region. The cities of Puyallup, Tacoma, Spokane, Pullman, and others have experimented with this class of permeable pavements as arterial roads, parking lots, sidewalks, pathways, and other applications (City of Tacoma, no date; Palmer, 2016). Permeable pavements are in-situ stormwater drainage systems that can reduce the overall cost of road construction projects by eliminating the need for stormwater ponds, piping, and drainage systems. While this class of pavements offers great ecological advantages, it is crucial to ensure that these pavements are safe for drivers and pedestrians, given the adverse winter conditions of the PNW.

Because of the porous nature of PC, this class of pavement can exhibit different icing patterns than traditional, non-permeable pavements. One study by Wetland Studies and Solutions, Inc. showed that PC tends to ice more quickly than neighboring non-permeable pavements, as seen in figure 1.1 (Wetland Studies and Solutions Inc., 2013). The icing patterns of PC need to be understood so that proper ice and snow control treatments can be applied in a timely manner.
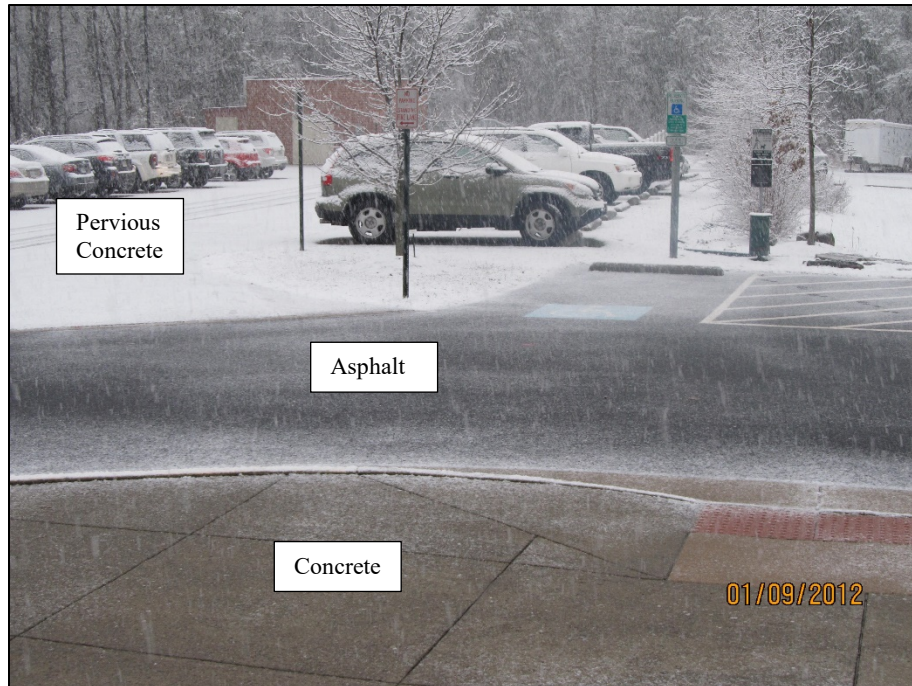
Figure 1.1. PCP versus traditional asphalt and concrete pavement during winter conditions (Wetland Studies and Solutions Inc., 2013)

Ice and snow control operations used to ensure safety and mobility on PCP during winter conditions are diverse and often selected on the basis of observation and experience, and they can contradict each other in different locations. The Urban Drainage and Flood Control District (UDFCD) recommended that liquid/solid deicers not be applied to PCP and that only mechanical snow removal be used (UDFCD, 2010). However, researchers reported that the removal of bonded ice layers from the PCP surface with plowing was more difficult than on traditional concrete because of the strong bond between the surface structure and the ice (Edens and Adams, 2001). In addition, stockpiling snow on PCP should be avoided, per the recommendations of the Washington State Stormwater Center for permeable pavements maintenance (Washington Stormwater Center, 2015).

Clogging of the air voids with debris can reduce the permeability of PCP and result in standing stormwater that forms an ice layer on the pavement surface and can cause safety

hazards during PNW winters (see figure 1.2). In addition, one of the main advantages of PCP over conventional concrete is skid resistance due to a rougher surface. Clogging of voids may also affect PCP skid resistance, which is significantly needed during icy conditions (Rodin III *et al.*, 2019). When PCP voids are clogged, vacuum- sweeping of PCP installations is typically carried out to restore permeability. However, vacuum-sweeping typically requires third-party contractors and also requires roadway closure. Therefore, a simple method is required to classify the levels of clogging and the in-situ volumetric porosity of PCP to determine at which level and how frequent vacuum-sweeping is required.
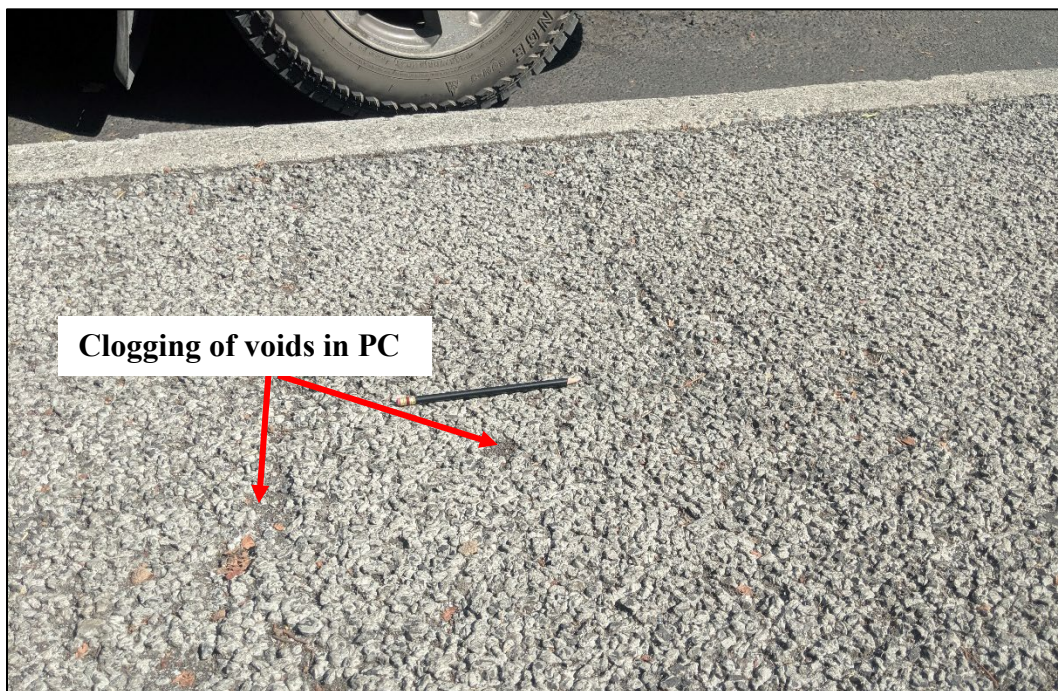
Figure 1.2 A PC sidewalk with clogged voids

A PC's performance (e.g., infiltration rate) is largely dependent on its porosity. The skid resistance of PC can also depend directly or indirectly on porosity and ice formation rate. However, a simple and non-destructive method to determine the in-situ porosity of PC currently

does not exist. The current submersion method (ASTM C1754) (ASTM, 2012) requires extraction of a core specimen from the pavement, which is destructive and costly and requires road closure.

1.2. <u>Scope of Work</u>

A literature review was performed to find available image-based methods applicable to PC for porosity characterization. Then, a non-destructive image-based method was developed to quantify the porosity of 27 laboratory-cast slabs cast at low, medium and high levels of porosity. In this method, the surface pores detected by image processing photographs taken with consumer-grade digital cameras were used to quantify the slabs' porosity. The results were corelated with the porosity results from the ASTM C1754 method commonly used on laboratory and field cores. For validation, cores were extracted from the slabs and scanned with X-ray computed tomography. The distribution of pores throughout the depth was quantified with image analysis of the X-ray CT images. These results were then compared to those obtained with the surface imaging method to study the impact of vertical distribution of pores on the results of the developed method. Furthermore, the infiltration rate of all the PC slabs was obtained, and a relationship between the porosity and infiltration rate of PC was developed.

To evaluate the effect of in-situ conditions such as clogging on the skid resistance of PC, the British Pendulum Tester (BPT) was used at several PC sites on the Washington State University (WSU) Pullman campus. Experimental testing of laboratory-cast PC slabs was conducted to correlate the surface pores and skid resistance of PCP with porosity so that in-situ porosity can be estimated on the basis of the developed correlations.

An essential step in establishing a winter maintenance protocol for PCP is to understand the icing pattern of the pavement, which requires an ice formation model based on ambient

4

temperature and pore size distribution in PCP. In this study, a validated model used in previous studies on conventional concrete was proposed to predict the temperature at which ice formation starts in PC. The potential applications of this model on PC require further research.

CHAPTER 2.   Literature Review on Pervious Concrete Porosity Characterization

The pore structure of PC can be effectively analyzed by using image analysis techniques. One of the powerful imaging tools is X-ray computed tomography (X-ray CT). With the X-ray CT approach, an X-ray beam is sent to infiltrate the PC sample from different angles and the data are collected in a flat-panel scintillator detector. After that, image analysis software is used to reconstruct a three-dimensional (3D) image from the multiple 2D images, as seen in figure 2.1 (Bordelon and Roesler, 2014).
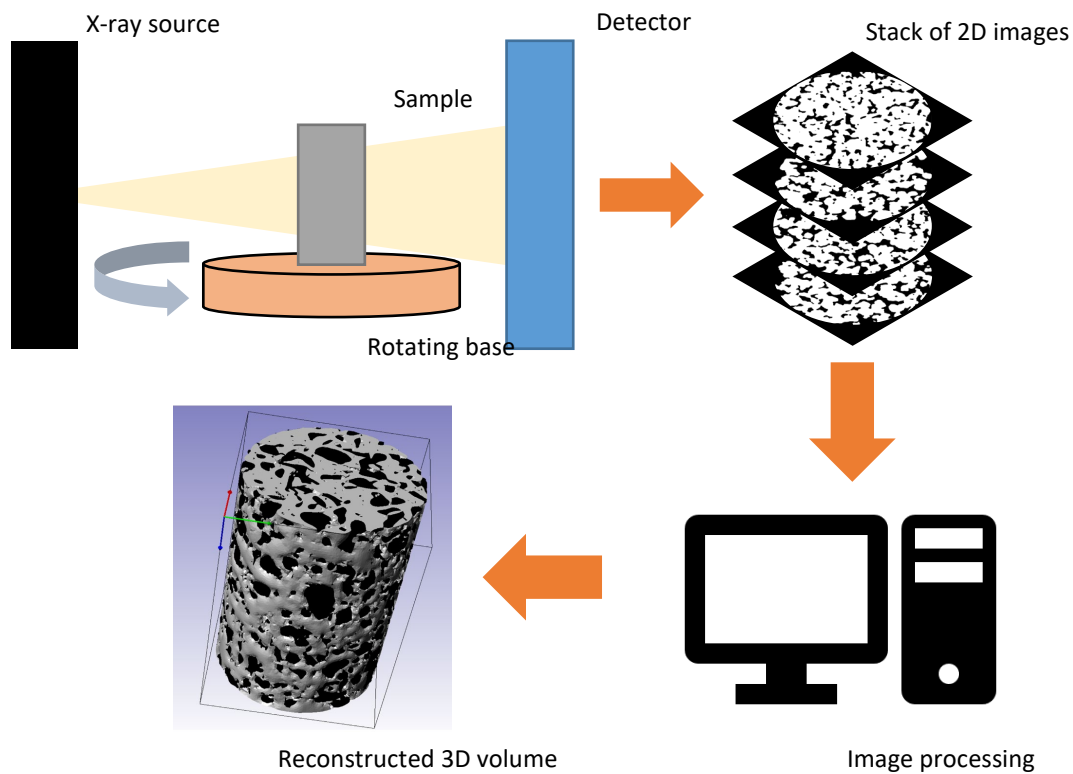
Figure 2.1 X-ray CT imaging procedure.
Recreated from Ying et al. (2013) and Bordelon and Roesler (2014)

Chandrappa and Biligri (2018) used X-ray microcomputed tomography (micro CT) to study the pore structure of pervious concrete. VGStudio MAX software was used to reconstruct three-dimensional (3D) images for all PC samples from 2D images captured by X-ray CT. Image

histograms were also used to isolate voids from solids and measure planner porosity. The

resulting porosity from X-ray CT matched well with the volumetric porosity obtained from the

ASTMC1754 (ASTM, 2012) test on pervious concrete samples, as shown in figure 2.2.
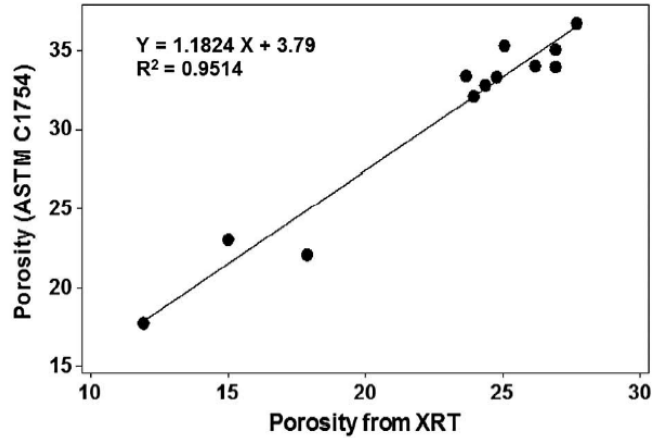
Figure 2.2 Comparison between porosity from X-Ray CT and ASTM C1754
(Chandrappa and Biligiri, 2018)

To investigate the effects of clogging on PC permeability, Kayhanian et al. (2012) used

X-ray CT to analyze PC cores (extracted from different parking lots in California) and construct

their porosity profiles using a stack of 2D images. Vertical and horizontal slices of 2D images

were also taken from the processed 3D image to build porosity profiles of the PC cores. The 2D

images were processed in MATLAB and ImagePro Plus to separate voids from solid particles

and obtain the void ratio. The authors found that clogging mostly occurred near the top surface

of PC pavement. Furthermore, the overall porosity of the cores determined by image analysis did

not correlate well with the porosity obtained by the gravimetric method (similar to the ASTM

C1754 method).

In a study by Neithalath, Sumanasooriya and Deo (2010), PC cylinders were cut into four

sections, and the top and bottom surfaces of each section were scanned to obtain 2D images. The

images were used to obtain the void area fraction for comparison with the specimen's volumetric porosity. The surfaces of PC sections were painted in white to easily separate voids from solids in the image processing software. Then the 2D images were cropped and transformed into binary images with ImageJ software. Using a threshold gray value, the voids were separated from solids, and the ratio of voids area to the total area was obtained for each sample. The relationships between the void area fraction of a 2D planner and the volumetric porosity of the PC samples from different mixtures are shown in figure 2.3. The variations between the void area fraction and volumetric porosity might have resulted from the fact that isolated voids were included in the calculation of porosity in the image analysis while the volumetric porosity represented only interconnected voids (Neithalath, Sumanasooriya and Deo, 2010).
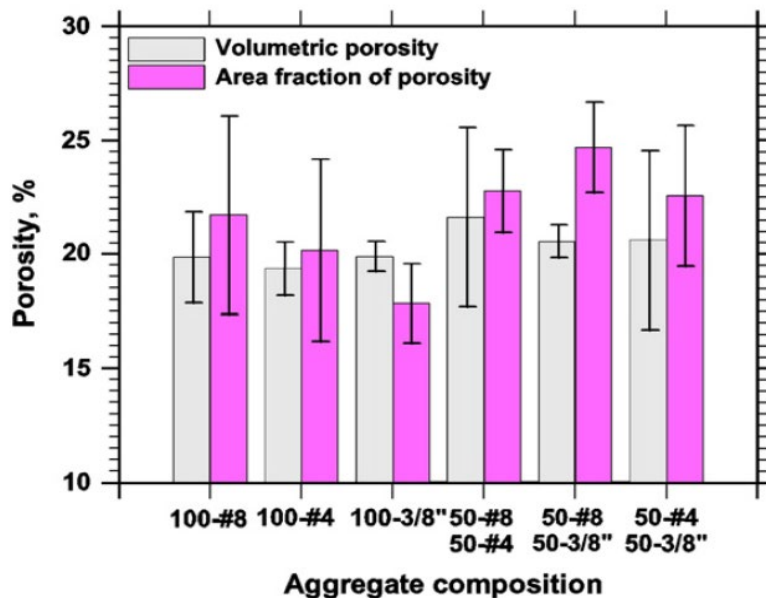
Figure 2.3 Comparison between porosity and void area fraction of PC samples from different mixture designs

As part of their study of water flow through PC, Zhang *et al.* (2018) compared the porosities of twelve 100-mm PC cubes obtained with the water displacement method (similar to the ASTM C1754 method) and X-ray CT. The twelve cubes were divided into four groups in

which each group had different porosity levels of 10, 15, 20, and 25 percent. 2D slices were

obtained at each 0.1 mm along the vertical of each specimen. The PC reconstructed model

(100x100 mm - 1000x1000 pixels) was cropped into 40x40-mm cubes to reduce the

computational analysis time. The 3D pore structure of PC was obtained with the watershed

segmentation algorithm, as seen in figure 2.4. After that, the ratio of the volume of voids to the

total volume could be calculated. The connected voids that allow for water infiltration could also

be calculated from the 3D model as the effective porosity. Another method to obtain porosity is

to use the 2D slices from CT imaging to calculate the area fraction of voids. Because the area

fraction of voids can change along the vertical direction of the sample, the average planner

porosity of 21 slices for each sample at equal spacing was reported for each sample. Zhang *et al.*

(2018) presented a comparison between the target, experimental, planner, 3D, and effective

porosity of the four groups of PC, as shown in figure 2.5.
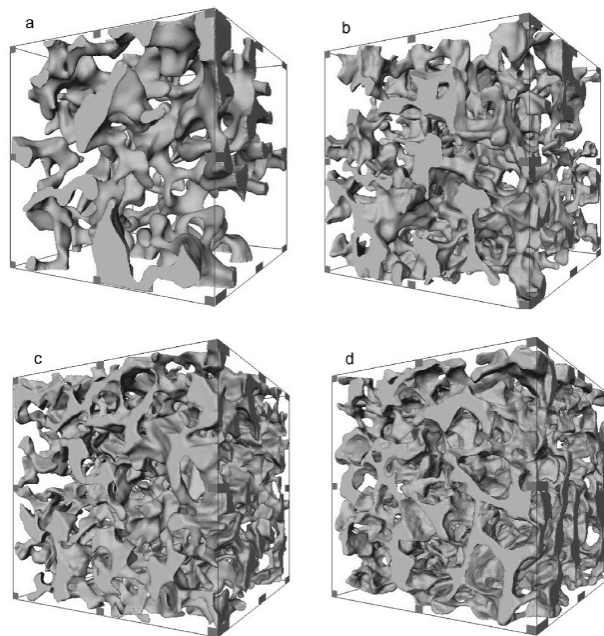
Figure 2.4 3D pore network of specimens from four porosity levels: a) 10 percent; b) 15 percent; c) 20 percent; d) 25 percent (Zhang *et al.*, 2018)

10
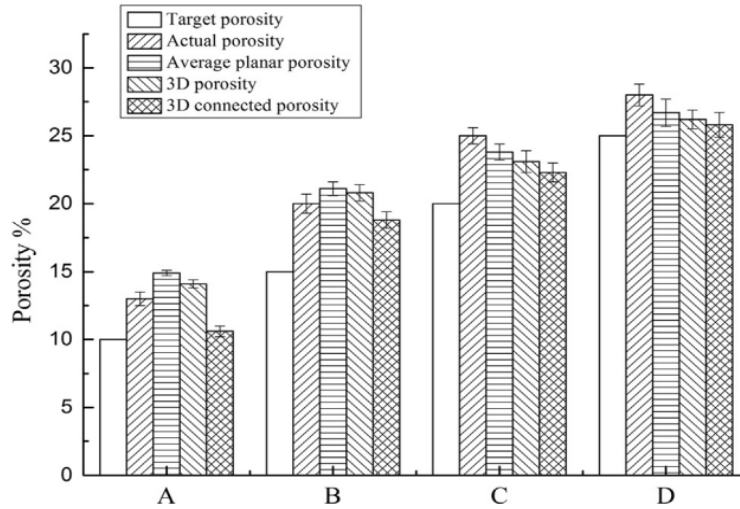
Figure 2.5 Comparision of PC porosity measured with various methods.

Pore size can also be determined from 2D CT images by using ImageJ software. Zhang et al. (2018) used the equivalent elliptical fitting method to describe pore size. The process started with segmentation using a specific threshold value in ImageJ to extract the actual pore shapes. After that, elliptical shapes were fitted to obtain the size and number of voids in each slice.

In all the reviewed literature, the volumetric porosity of in-situ PC could not be determined unless cores were extracted and tested in the laboratory. This research proposed a new method to estimate the volumetric porosity via simple photography and image processing techniques.

CHAPTER 3.   Materials and Methods

In a previous PacTrans project by the Principal Investigator (PI), 27 PC slabs measuring 10×10×3.5 inches were cast at three porosity levels: low (15 percent), medium (25 percent), and high (35 percent). For each porosity level, nine slabs were cast. The PC slabs were made with crushed basalt aggregates commonly used in eastern Washington state. The particle size distribution of the aggregate and the PC mix design are shown in figure 3.1 and table 3.1.
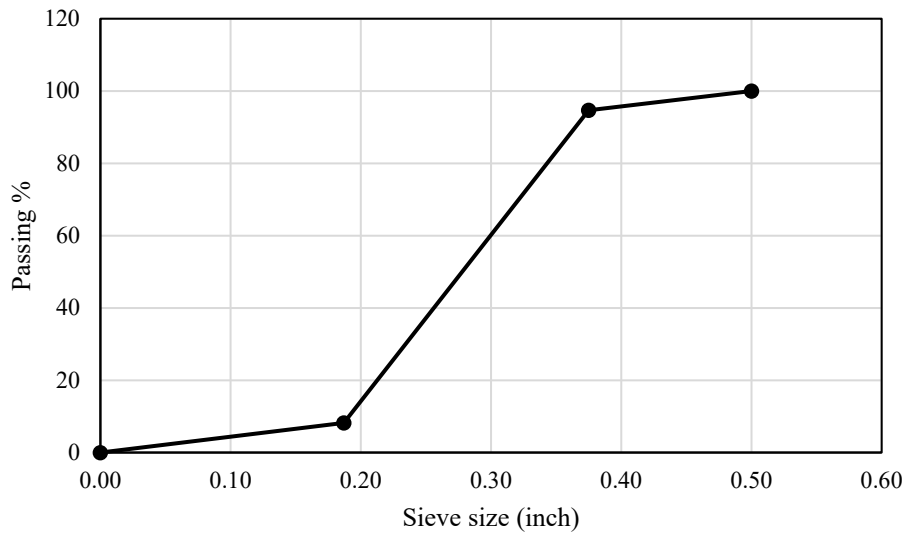
Figure 3.1. Particle size distribution of the coarse aggregates used in the PC mixture

Table 3.1 PC mixture design

Material	Proportion
Coarse aggregate (lb/yd^3)	2,319
Cement Type I/II (lb/yd^3)	697
Water content (lb/yd^3)	189
Water/cement	0.30
VMAR (water reducer) (oz/100 lb of binder)	8.0
Recover (hydration retarder and stabilizer) (oz/100 lb of binder)	7.9
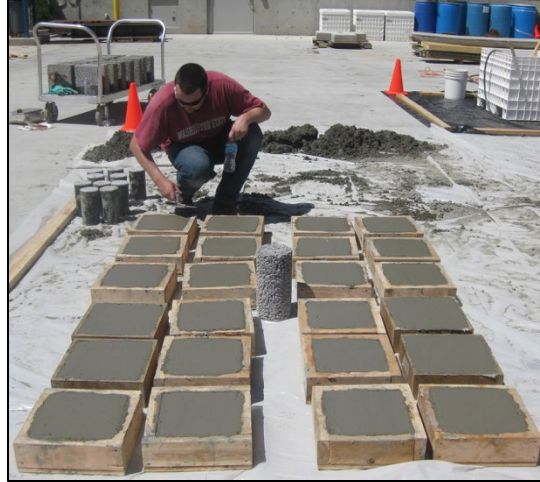
Figure 3.2. The WSU team casting slabs for the PacTrans project

3.1. Measuring Porosity with the Submersion Method

The porosity of the PC specimens was measured experimentally following the procedure described in ASTM C1754 (ASTM, 2012). This method is commonly used for laboratory-cast specimens or field cores. So it was important to correlate this test's results with the results obtained from the non-destructive, image-based method in this study.

First, specimens' dimensions were recorded to calculate the volume (V). Specimens' diameter and height were taken as the average value of two caliper measurements. Then, the dry weight of each specimen (M_d) was measured. Next, each specimen was submerged in water for 30 minutes and the submerged mass (M_W) was recorded. Finally, porosity (P) was calculated by using Equation 1. See figure 3.3 for the test set-up.

$$P = [1 - \left(\frac{M_d - M_w}{\rho_w * V}\right)] \times 100 \qquad \text{Eq. 1}$$

Figure 3.3. Water bath for submerging specimens for porosity testing

The porosity results of all the tested slabs are shown in figure 3.4. All the slabs achieved porosities close to the targeted porosity levels (15, 25, and 35 percent).
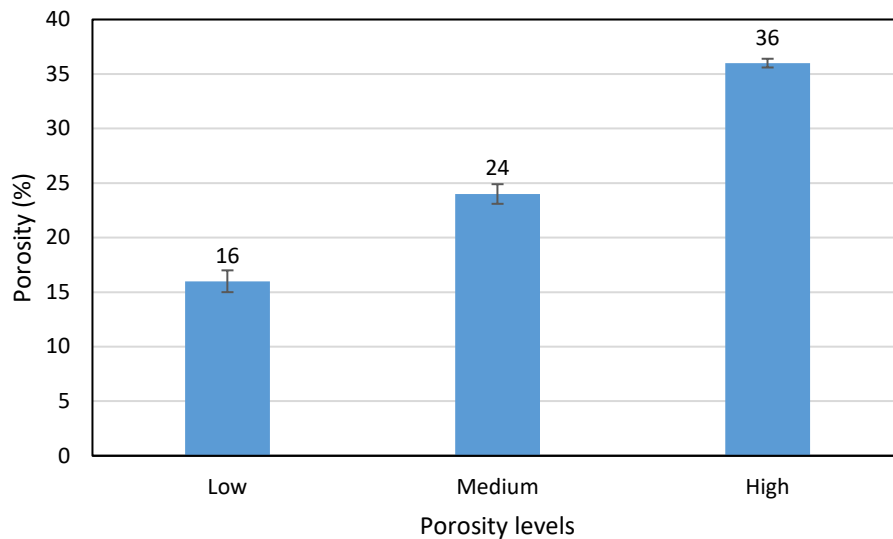
Figure 3.4 Porosity results for all PC slabs (measured according to ASTM C1754)

These results were then used, as described in the next section, to correlate with the porosities obtained with the non-destructive image-based method.

CHAPTER 4.   Characterization of Porosity by Surface Photography

In an attempt to obtain porosity with a simple, image-based method rather than the with the ASTM C1754 (2012) method described in the previous chapter, image analysis of the surfaces of all the slabs was performed. The top and bottom full faces of each slab were photographed with an 8-megapixel camera, and the photographs were converted into binary images. After that, image binarization was performed with the ImageJ software (Ferreira and Rasband 2012), in which a specific threshold was applied to isolate the background (air voids) from the foreground (solid part) in the image, as seen in figure 4.1. When a pixel value was higher than the threshold value, it was counted as the foreground and vice versa. The image-based porosity was calculated as the ratio of the void area to the total surface area of the slab.
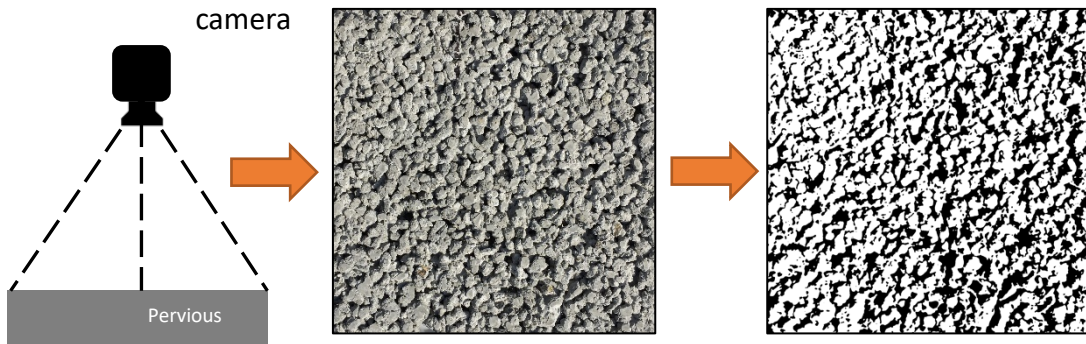
Figure 4.1 Image binarization using ImageJ software

The image-based porosity results of the top and bottom surfaces of all the slabs in each porosity level (low, medium, and high) were compared with the porosity obtained with ASTM C1754. Figure 4.2 shows that the image-based porosity was generally higher than the porosity obtained with the ASTM C1754 method. A difference between the results from the two methods was expected because the ASTM C1754 method only yields the open and connected pores that

allow the water to enter whereas the image-based method included all the pores (connected, isolated, and dead-end channels). Furthermore, the imaging was only conducted at the top and bottom, whereas the fractal area of the pores varied at intermediate depths, described as the tortuosity of the 3D interconnected pore system. The effect of the variation of pore distribution through the depth will be further discussed in Chapter 5.

As shown in figure 4.2, for high-porosity slabs, the two methods showed closer agreement, as the image-based porosity was 14 percent higher than the submerged porosity. For low-porosity slabs, the image-based porosity was 119 percent higher than the submerged porosity. This observation may have been due to the high compaction energy applied to multiple layers of the fresh PC during the casting of low-porosity slabs, resulting in fewer voids at the intermediate depths than at the surface. Therefore, correlating image-based porosity with submersion-based porosity was found to be more effective for PCPs with high volumetric porosity.
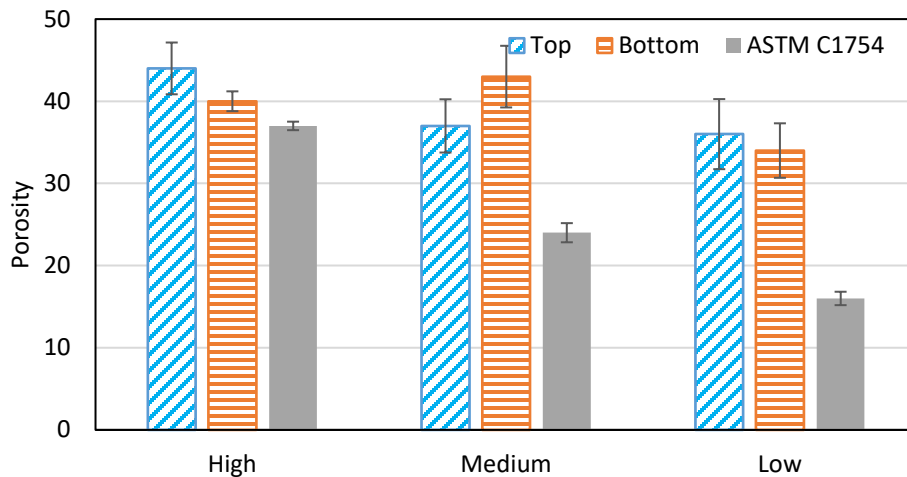
Figure 4.2 Comparing the image-based porosity of the top and bottom surfaces of PC slabs versus ASTM-C1754 porosity

To establish a correlation between image-based top porosity and ASTM-C1754 porosity, the average image-based porosity of the top surfaces of all PC slabs were plotted against the average slabs' ASTM-C1754 porosity results as illustrated in figure 4.3. With a coefficient of determination value of 93 percent, the figure shows that a correlation between image-based porosity and ASTM-C1754 porosity existed. However, the surface porosity was always higher than the ASTM-C1754 porosity.
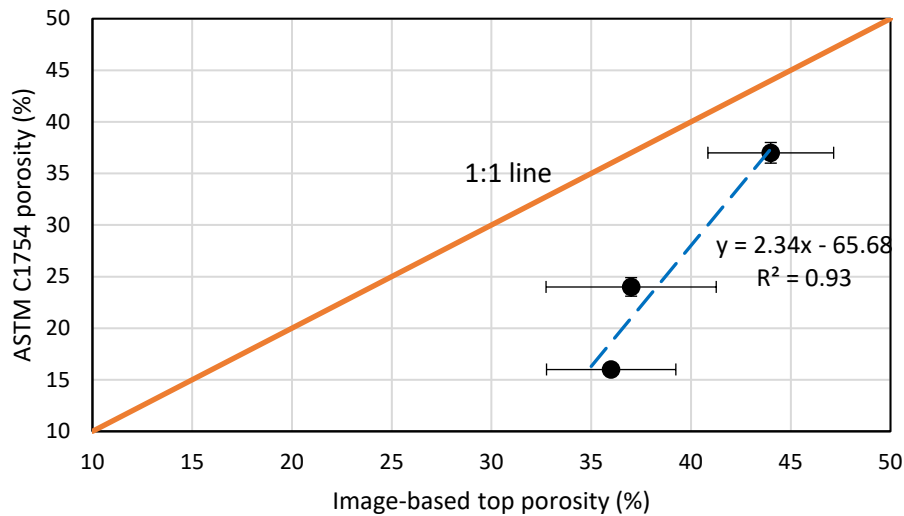
Figure 4.3 Correlation between ASTM-C1754 porosity and image-based top porosity of PC slabs

On the basis of the data from 27 slab, a regression-based model was derived to obtain the ASTM-C1754 porosity of PC slabs based on the image-based top porosity, as seen in Eq. 2 (R^2=86 percent).

$$\text{ASTM-C1754 porosity} = 2.34 \cdot \text{top surface porosity} - 65.68 \qquad \text{Eq. 2}$$

Therefore, the use of a consumer-grade camera and image processing software will allow the ASTM-C1754 porosity of in-situ PCP to be obtained by using the proposed model in Equation 1. In addition, the proposed approach can be used to monitor the clogging of voids in in-situ PCP

over time. Note that Equation 1 is applicable only to PC with basalt aggregates that have a particle size distribution similar to that shown in figure 3.1. Testing of more specimens with varied porosity, aggregate, and mix formulation will be required to increase the reliability and applicability of the developed approach.

CHAPTER 5.   Porosity Characterization by X-ray Computed Tomography

To further explore the pore structure of PC and to study the effect of vertical pore distribution on the developed method, X-ray computed tomography (X-ray CT) and image processing techniques were employed. X-ray CT, which offers valuable insight into the internal macrostructure of PC without destructing the specimen, was carried out on three PC cores extracted from the same slabs, with three porosity levels: low (14 percent), medium (20 percent), and high (33 percent). The specimens are shown in figure 5.1.

| Low | Medium | High |
| P = 14% | P = 20% | P = 33% |
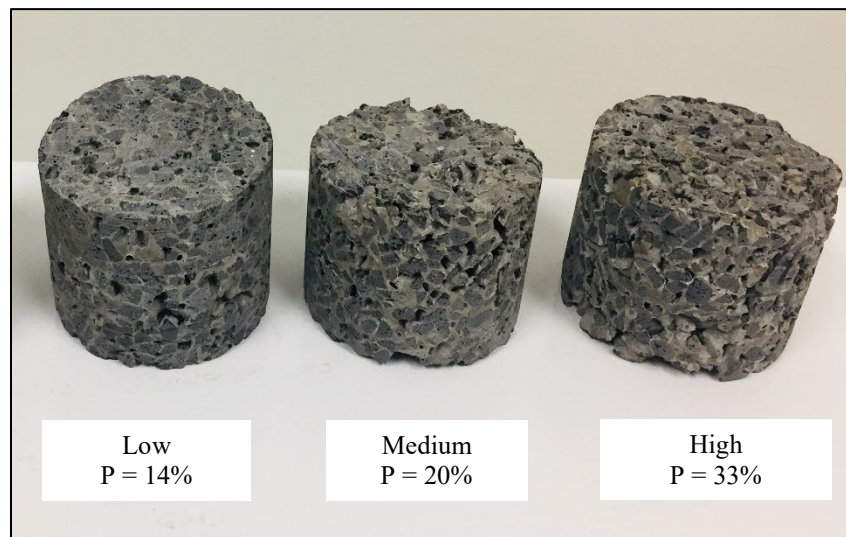
Figure 5.1 PC cores with varying porosity levels

An X-ray CT machine at the University of Washington was used to scan the three PC samples and obtain planner images (slices) at different positions along the vertical axis, as illustrated in figure 2.1 and figure 5.2. About 1600 images were acquired by X-ray CT scanning of each specimen.
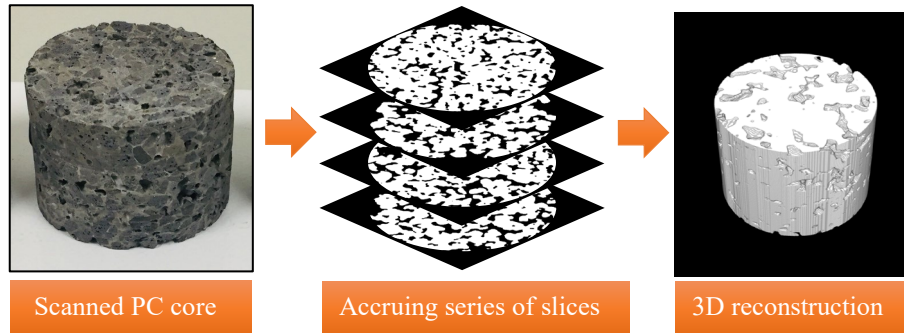
Figure 5.2 Imaging PC samples using X-ray CT

The raw images were then cropped to 400×400-pixel square images to avoid edge effects during the analysis process. Using ImageJ software, the cropped images were binarized with the Otsu thresholding technique to isolate the voids from the solids on the basis of the pixel values. When the pixel value was lower than the assigned threshold, it was then counted as a void and changed to zero (black color) and vice versa. Moreover, the binarized slices were used to reconstruct a 3D image of the scanned PC sample (figure 5.2) with the MATLAB image processing toolbox, and the overall porosity was obtained.

The porosity of the cores was also measured experimentally following the ASTM C1754 submersion method, as discussed in Section 3.1. The test results indicated that the cores' ASTM-C1754 porosities varied from 14 percent to 33 percent. The porosity results obtained experimentally by ASTM C1754 and using X-ray CT images were in good agreement, as seen in figure 5.3. This agreement shows that most of the pores in these cores were reached by the water.

2
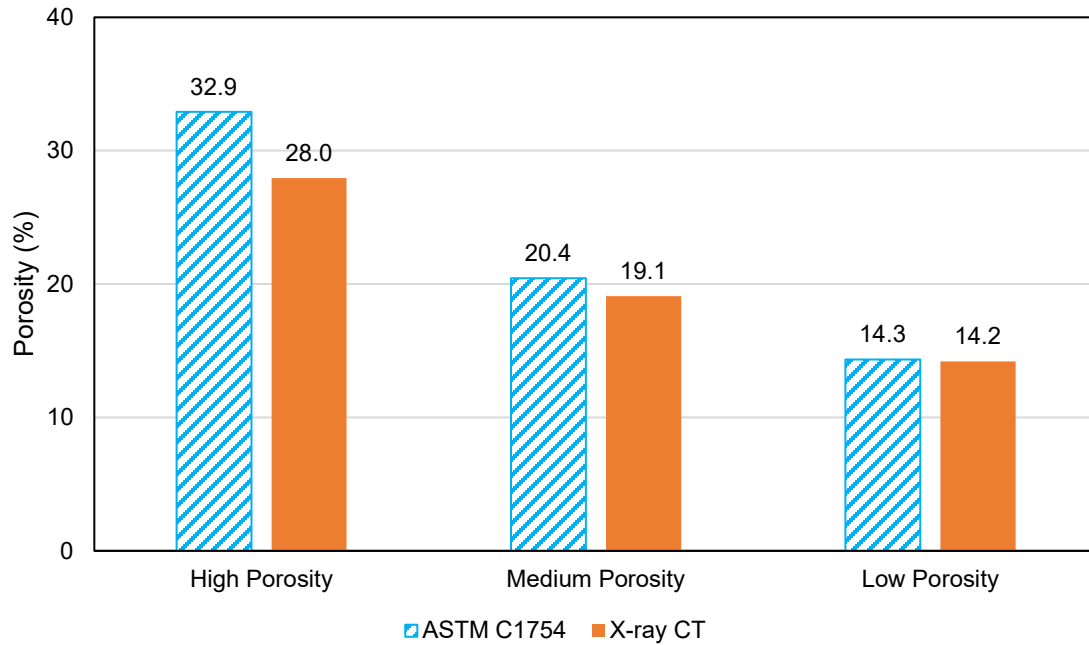
Figure 5.3 Comparing porosities obtained experimentally (ASTM C1754 by submersion) and with image analysis of X-ray CT images

Next, the image-based porosity (void area divided by the total area) of all the slices for each core was obtained by using ImageJ. For instance, at a depth of 1 inch, the binarized images and the image-based porosity (area fraction) of a slice at the cross-section of each specimen are illustrated in figure 5.4. It can be observed visually that the areas of voids (black areas) were larger for higher porosity samples.

| Low (Areal P= 9.5%) | Medium (Areal P= 24%) | High (Areal P= 34%) |
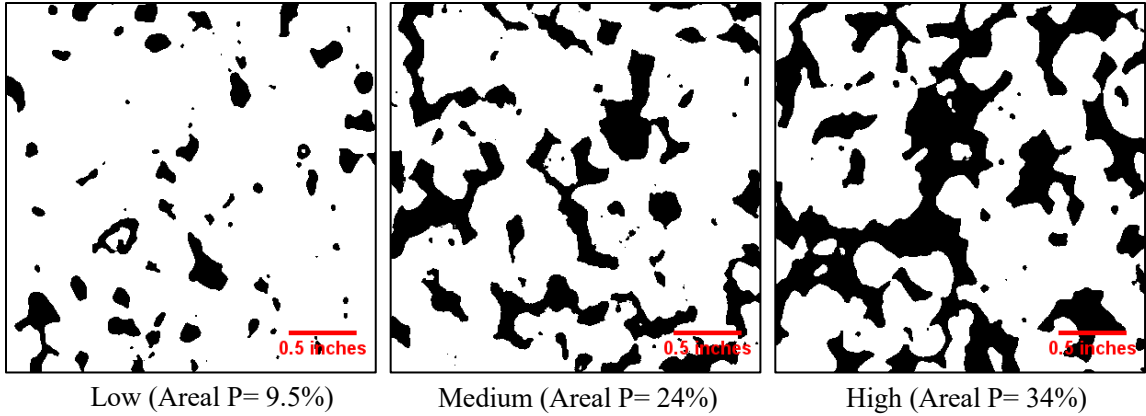
Figure 5.4 Binarized images of X-ray CT slices obtained at 1-inch depth for each PC core

This analysis was repeated for each slice. The image-based porosity results were plotted along the depth, as seen in figure 5.5 to study the porosity distribution for each PC core.

$$y = 5E\text{-}05x^2 - 0.2073x + 4.7308$$
$$R^2 = 0.8319$$

$$y = -0.0012x^2 - 0.0933x + 5.2075$$
$$R^2 = 0.5909$$

$$y = 0.0017x^2 - 0.197x + 4.8219$$
$$R^2 = 0.764$$

× high (P=33%)
▲ Medium (P=20%)
● Low (P=14%)
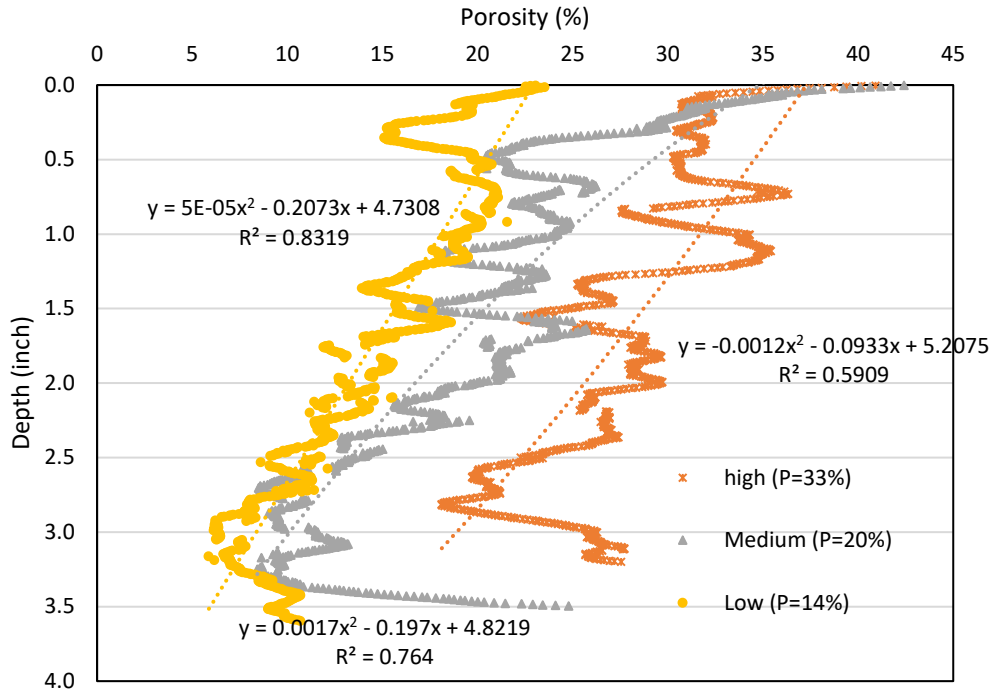
Figure 5.5 Porosity variation along the depth of each specimen base on X-ray CT scans. The ASTM-C1754 porosity (P) is provided in the legend for each specimen

4

The results from figure 5.5 illustrate that porosities at the top and bottom surfaces (the first and last 0.5 inch) were higher than the porosity of the intermediate depths for all the PC cores. This explained the difference between the image-based and the ASTM C1754 porosity results. As previously seen in figure 4.2 and figure 4.3, the results from the photography method corresponding to the top and bottom surfaces of the PC slabs were always higher than the overall porosity obtained by the ASTM C1754 method. For cores with high and medium porosity, minimal compaction was applied to the fresh PC surface; hence, the image-based porosity was found to be similar to the ASTM-C1754 porosity, as discussed in Chapter 4. However, to achieve low porosity, fresh PC was placed in layers, and each layer was compacted. This procedure resulted in greater compaction to the intermediate layers than to the surface layer, which means higher porosity at the surface layers than at mid-depth layers (figure 5.5). Therefore, large discrepancy between image-based porosity and the ASTM-C1754 porosity was observed for slabs with low porosity (figure 4.2).

CHAPTER 6. Effect of Porosity on the Infiltration Rate of Pervious Concrete

The infiltration rate of the slabs was measured following a modified version of the ASTM C1701 procedure (ASTM, 2017). An amount of 0.26 gallon (one liter) of water was poured into a 4-inch-diameter ring placed on the slab surface, and the bottom edge of the ring was sealed with plumber's putty so that water flowed only through the PC slab. The water head was kept constant at 0.6 inch (15 mm), and the time it took the 0.26 gallon of water to infiltrate through the slab was measured. The test was repeated at four locations for each slab, with three trials at each location (only the last two repeats were recorded, while the first trial was for wetting the specimen). The average value of the four repeats was reported for each slab. The infiltration rate was calculated as shown in Eq. 3.

$$I = \frac{KM}{D^2 t} \qquad\qquad \text{Eq. 3}$$

where I is the infiltration rate (inch/hour), M is the mass of water, D is the inner diameter of the ring, t is the time required for the water to infiltrate, and K is a conversion factor equal to 126,870 inches. The infiltration results for all the slabs were plotted against the ASTM-C1754 porosity, shown in figure 6.1.
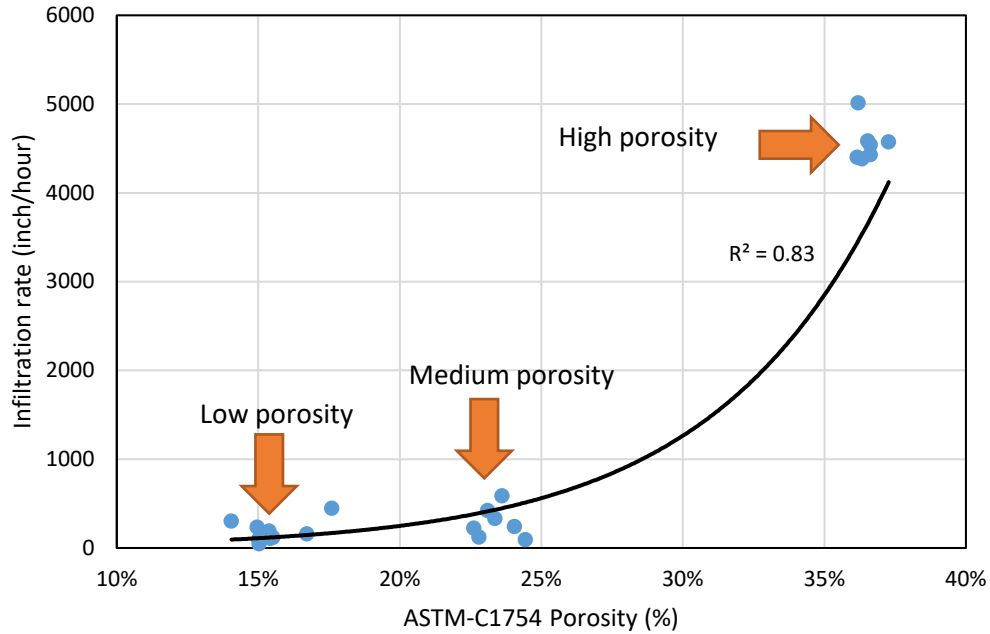
Figure 6.1. Infiltration rate results for all PC slabs

Figure 6.1 shows that the infiltration rate increased exponentially with an increase in porosity. A correlation between infiltration rate and ASTM C-1754 porosity can be obtained from the results in figure 6.1, as shown in Equation 4.

$$P = \frac{\ln\frac{I}{9.657}}{16.249} \qquad\qquad \text{Eq. 4}$$

where P is ASTM-C1754 porosity, and I is the infiltration rate in inch/hour. The correlation shown in Equation 3 is based on 23 samples with an R^2 value of 0.83. The in-situ infiltration rate can be used in the field to estimate in-situ porosity.

CHAPTER 7. In-situ Skid Resistance Evaluation of Pervious Concrete Pavements

In a previous PacTrans project by the PI, the skid resistance of laboratory-cast PC slabs was measured by using the British Pendulum Tester (BPT). In the current project, the BPT method was used to evaluate the in-situ skid resistance of five PCPs at Washington State University's Pullman campus to study the effect of clogging and age. The type, age, and surface conditions of the tested PCPs are presented in table 7.1. The tested pavements included the following locations:

1. PACCAR Environmental and Technology Building's pervious concrete backyard
2. Veterinary Hospital parking entrance
3. Community Hall sidewalk
4. Sloan Hall sidewalk
5. Valley Playfield east sidewalks

Table 7.1 Conditions of the tested PCPs on WSU's Pullman campus

Location	Pavement Type	Age at the time of testing	Ravelling	Clogging	Polished Aggregate
Pervious Concrete Pavement (PCP)					
1	Parking lot	4 years, 2 months	No	No	low
2	Driveway entrance	unknown	High	High	Moderate
3	Sidewalk	4 years, 3 months	Low	No	No
4	Sidewalk	unknown	No	High	No
5	Sidewalk	8 years, 11 months	No	No	Moderate

The BPT test was conducted on the tested PCPs in accordance with ASTM E303 (ASTM, 2013) (figure 7.1). The BPT test was repeated four times at each test location to obtain representative results. Furthermore, two rubber sliders were used for each BPT test, a Pedestrian Slip Rubber (PSR) (CS-PEND-855/1070) and a Tire Slip Rubber (TSR) (CS-PEND-855/1060).

9

The tests were run at each test location under dry and wet conditions. The average BPN values of all the tested locations under dry and wet surface conditions are presented in figure 7.2. It can be observed that the skid resistance of PCP for pedestrian users (tested with the PSR slider) was not significantly affected by surface conditions (except for location 5, where the BPN of the wet condition was 33 only less than the BPN of the dry condition). However, the skid resistance of the PCP for vehicles (tested using the TSR slider) in wet conditions was, on average, 29 only less than that of the dry condition (Figure 7.2). This suggests that the infiltration capacity of PC should be always maintained to ensure that stormwater is fully infiltrating the pavement and that no water is ponding on the pavement surface.
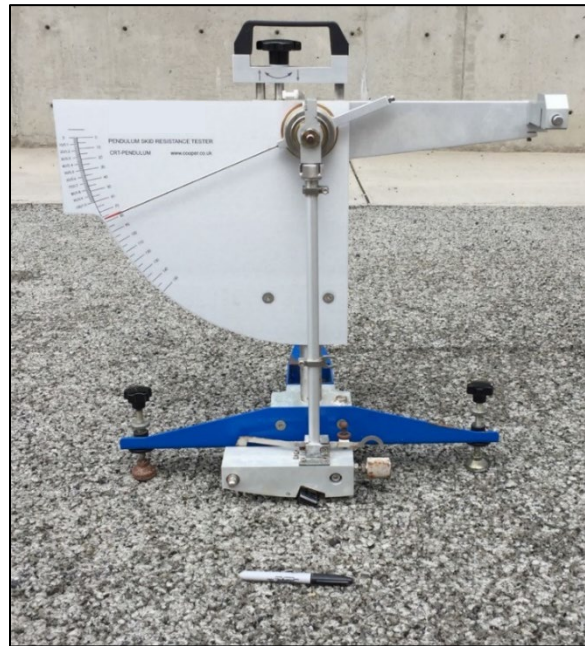
Figure 7.1 In-situ skid resistance testing of PCP using the BPT at location 1
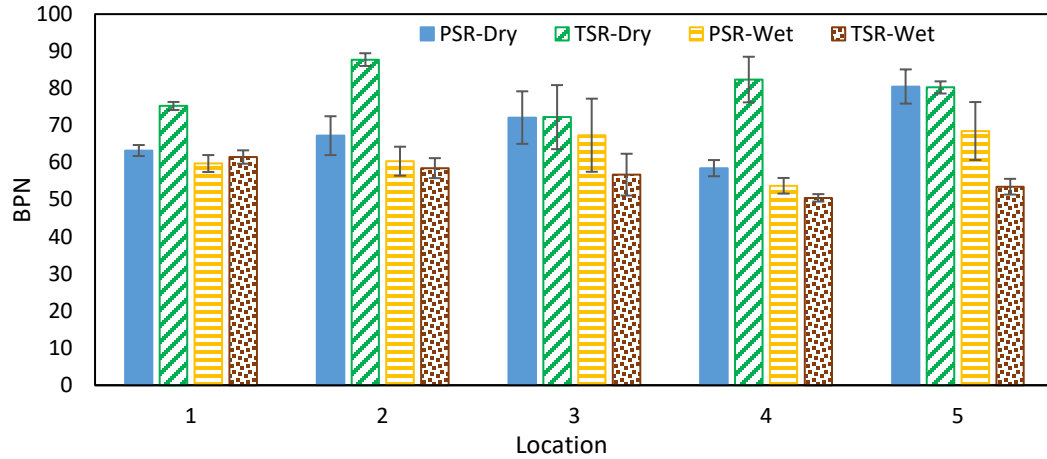
Figure 7.2 In-situ average BPT test results under dry and wet surface conditions
(Rodin III *et al.*, 2019)

In the previous PacTrans project by the PI, the skid resistance of lab-cast PC slabs with various porosity levels (16-36 percent) was measured with the BPT. Figure 7.3 illustrates the effect of porosity on the BPN values under different surface conditions. It was concluded that the effect of porosity on the skid resistance of PCP measured with a BPT was statistically insignificant (Rodin III *et al.*, 2019). Therefore, further research is required to identify a different method to evaluate the in-situ porosity of PCPs.
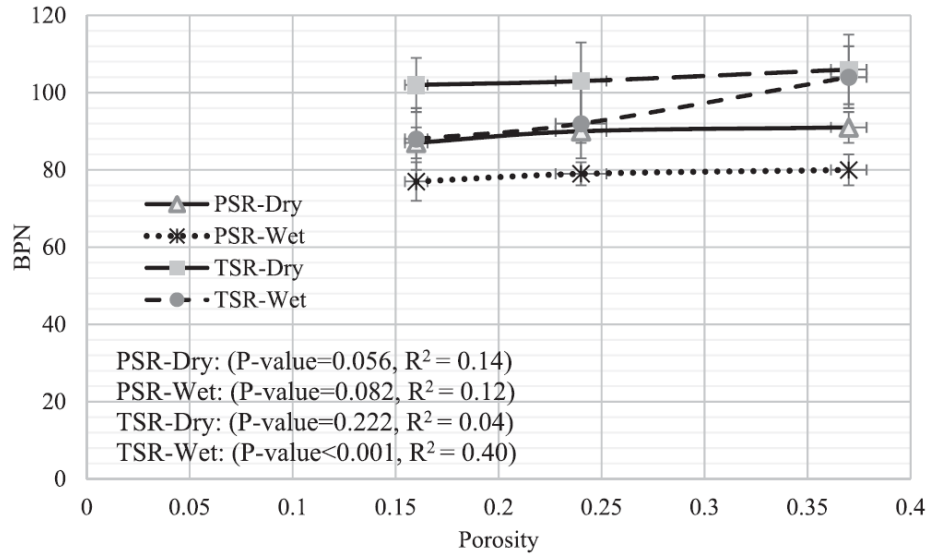
Figure 7.3 Effect of porosity on the skid resistance of PC (Rodin III *et al.*, 2019)

CHAPTER 8.   Application of a Frost Model for Pervious Concrete

One of the most important goals of studying freezing effects on PC is to determine the temperature at which ice will start to form in the cement paste pores. Obtaining the ice-formation temperature will help transportation agencies to develop a winter maintenance protocol so that deicing treatments can be applied to the pavement only when the risk of freeze-thaw damage is anticipated. A well-known method for obtainin the ice formation temperature threshold is the thermodynamic-based Gibbs-Thompson model (Coussy and Monteiro, 2008; Liu *et al.*, 2011; Ng and Dai, 2014; Gong *et al.*, 2015):

$$T_m(K_{CL}) = T_m(0) - \frac{\gamma_{CL}K_{CL}}{\Delta S_{fv}}$$
<div align="right">Eq 5</div>

where:

T_m: Threshold temperature for ice formation in a spherical pore with a radius = r_p

$T_m(0)$: Melting point (273 K for ice)

γ_{CL}: Crystal-liquid interfacial energy (~ 0.0409 J/m^2)

K_{CL}: $2/(r_p - d_W)$:Curvature of the crystal-liquid interface related to a spherical pore radius

(r_p)

d_W: Thickness of unfrozen water layer which is approximately 0.9 nm for water

ΔS_{fv}: Molar entropy of fusion, which equals $(S_L - S_C)/v_C$ where S_L and S_C are the molar entropies of the liquid and ice crystal and v_C is the molar volume of the crystal. ΔS_{fv} for ice is ~1.2 MPa/K

Several studies successfully applied the Gibbs-Thompson equation to model freeze-thaw damage in cement paste. Ng and Dai (2014) used the Gibbs-Thompson equation to develop and

validate a model for fracture of cement paste due to internal frost damage. The pore network of the cement paste was digitally reconstructed with scanning electron microscopy (SEM) and used as the geometry for a 3D cohesive zone fracture model. The internal pressure at the pore scale that was induced by ice formation was calculated on the basis of the Gibbs-Thompson equation and thermodynamic energy balance. The material response to the frost-induced pressure was modeled and validated with experimental results. In addition, Liu *et al.* (2014) developed a numerical model to predict frost damage in cement-based systems. As part of the developed model, the Gibbs-Thompson equation was used to calculate the temperature threshold at which pore water freezes. The model was successfully validated with experimental results. On the basis of the reviewed studies, application of the Gibbs-Thompson equation for PC frost development to determine the critical temperature at which maintenance (such as deicing chemical application) should be performed on PCP shows promise and should be studied.

CHAPTER 9.   Conclusions

This study aimed to develop a simple, image-based method to characterize the porosity of PC. Pervious concrete porosity was characterized with three methods: the submersion method based on ASTM 1754, surface imaging using photography and image processing tools, and X-ray computed tomography (X-ray CT). In addition, the British Pendulum Tester (BPT) was used to test the in-situ skid resistance of five PCPs on Washington State University's Pullman campus. On the basis of the results of this study, the following conclusions can be drawn:

- The porosity results from the surface imaging showed a strong correlation with the porosity results from submersion using the 27 tested PC slabs at three porosity levels (nine slabs for each level): 15 percent, 25 percent, and 30 percent. The image-based method consistently provided a higher porosity, as expected. This may have been due to the tortuosity of the 3D pore network, which would result in a different fractal area of voids in intermediate slices. It may also have been due to the dead-end channels and isolated pores that did not allow the water to enter in the submersion method. Testing of more slabs could help strengthen the developed correlation and establish a margin of error to account for the inherent differences between the two methods.

- Results from the analysis of X-ray CT images and the distribution of porosity along the depth of the slabs showed that the top and bottom 0.5-inch layers had higher porosities than the porosity at intermediate depths. Therefore, characterization of in-situ porosity using only images of the top surface was found to be unrealistic at this time. Imaging of more slabs in parallel with X-ray CT scans could help in developing models to describe the porosity distribution.

1

- The In-situ skid resistance of PCP, measured with the BPT, was found to be less in wet surface conditions than in dry conditions. Therefore, PCP should always be monitored to avoid clogging of voids and to ensure that the pavement is fully permeable and no stormwater is ponding on the surface in order to maintain high skid resistance.

In addition to the above-mentioned points, the Gibbs-Thompson model was proposed to identify the temperature at which ice formation starts in PC. This model can be a useful tool, based on the porosity level of PCP, to determine the critical temperature at which to apply deicing chemicals during cold weather.

In summary, the surface photography porosity method seems to have potential for characterizing permeable pavements. However, the top 0.5-inch of PC has a substantially higher porosity relative to the remaining depth. Therefore, surface imaging can result in unrealistic results for the overall porosity of the pavement. Here, the results of the method were discussed for use in winter maintenance. These porosity results could also be used to infer PC strength and mechanical performance, which is also difficult to characterize for in-situ pavement unless a core is extracted. The imaging method could also be used to quantify clogging and to apply sweeping on the pavement as needed.

References

ASTM (2012) *Standard Test Method for Density and Void Content of Hardened Pervious Concrete (ASTM C1754)*. West Conshohocken, PA,.

ASTM (2013) 'Standard Test Method for Measuring Surface Frictional Properties Using the British Pendulum Tester (ASTM E303)'. West Conshohocken, PA.

ASTM (2017) *Standard Test Method for Infiltration Rate of In Place Pervious Concrete (ASTM C1701/C1701M-17)*. West Conshohocken, PA.

Bordelon, A. C. and Roesler, J. R. (2014) 'Spatial distribution of synthetic fibers in concrete with X-ray computed tomography', *Cement and Concrete Composites*. Elsevier Ltd, 53, pp. 35–43. doi: 10.1016/j.cemconcomp.2014.04.007.

Chandrappa, A. K. and Biligiri, K. P. (2018) 'Pore Structure Characterization of Pervious Concrete Using X-Ray Microcomputed Tomography', *Journal of Materials in Civil Engineering*, 30(6), pp. 1–11. doi: 10.1061/(ASCE)MT.1943-5533.0002285.

City of Tacoma (no date) *Pervious Street Project*. Available at: https://cms.cityoftacoma.org/enviro/C118293Pervious St Project.pdf.

Coussy, O. and Monteiro, P. J. M. (2008) 'Poroelastic model for concrete exposed to freezing temperatures', *Cement and Concrete Research*, 38(1), pp. 40–48. doi: 10.1016/j.cemconres.2007.06.006.

Edens, M. Q. and Adams, E. E. (2001) *The Application of CT Technology to the Experimental Study of Highway Icing*. Civil Engineering Department, Montana State University.

Ferreira, T. and Rasband, W. (2012) ImageJ User Guide: IJ1.46r. http://imagej.nih.gov/ij/docs/guide

Gong, F. *et al.* (2015) 'Stress analysis for concrete materials under multiple freeze-thaw cycles', *Journal of Advanced Concrete Technology*, 13(3), pp. 124–134. doi: 10.3151/jact.13.124.

Kayhanian, Masoud & Anderson, Dane & Harvey, John & Jones, David & Muhunthan, Balasingam. (2012). Permeability Measurement and Scan Imaging to Assess Clogging of Pervious Concrete Pavements in Parking Lots. Journal of environmental management. 95. 114-23. 10.1016/j.jenvman.2011.09.021.

Liu, L. *et al.* (2011) 'Modeling of the internal damage of saturated cement paste due to ice crystallization pressure during freezing', *Cement and Concrete Composites*. Elsevier Ltd, 33(5), pp. 562–571. doi: 10.1016/j.cemconcomp.2011.03.001.

Liu, L. *et al.* (2014) 'Numerical investigation of the effects of freezing on micro-internal damage and macro-mechanical properties of cement pastes', *Cold Regions Science and Technology*. Elsevier B.V., 106–107, pp. 141–152. doi: 10.1016/j.coldregions.2014.07.003.

Neithalath, N., Sumanasooriya, M. S. and Deo, O. (2010) 'Characterizing pore volume, sizes, and connectivity in pervious concretes for permeability prediction', *Materials Characterization*. Elsevier Inc., 61(8), pp. 802–813. doi: 10.1016/j.matchar.2010.05.004.

Ng, K. and Dai, Q. (2014) 'Numerical investigation of internal frost damage of digital cement paste samples with cohesive zone modeling and SEM microstructure characterization', *Construction and Building Materials*. Elsevier Ltd, 50, pp. 266–275. doi: 10.1016/j.conbuildmat.2013.09.025.

Palmer, M. (2016) *Porous Pavement in Public ROW, Puyallup's Experience*, *Washington APWA chapter*. Available at: http://washington.apwa.net/Content/Chapters/washington.apwa.net/File/Conference Presentations%2FSpring 2016%2FRollerCompactedConcrete-PermeablePavements-S16.pdf.

Rodin III, H. *et al.* (2019) 'Evaluation of skid resistance of pervious concrete slabs under various winter conditions for driver and pedestrian users', *Road Materials and Pavement Design*. Taylor & Francis, pp. 1–19.

UDFCD (2010) *Urban Storm Drainage Criteria Manual, version 3*. Denver, CO.

Washington Stormwater Center (2015) *Permeable Pavements O&M, GENERAL: Snow Removal*, *Deparment of Ecology - State of Washington*. Available at: https://www.wastormwatercenter.org/files/library/module-54advanced-permeable-pavement-om1028141-slide.pdf.

Wetland Studies and Solutions Inc. (2013) *Winter Weather Considerations for Implementing Pervious Pavement*. Available at: http://archive.wetlandstudies.com/newsletters/2012/April/articles/PerviousPavementInWinter.html (Accessed: 13 December 2019).

Ying, H. *et al.* (2013) 'Heterogeneous finite-element modeling of the dynamic complex modulus test of asphalt mixture using X-ray computed tomography', *Journal of materials in civil engineering*. American Society of Civil Engineers, 26(9), p. 4014052.

Zhang, J. *et al.* (2018) 'Numerical study on seepage flow in pervious concrete based on 3D CT imaging', *Construction and Building Materials*, 161(February), pp. 468–478. doi: 10.1016/j.conbuildmat.2017.11.149.

Appendix A

Table A-1. Area fraction (%) of X-ray CT slices along the depth of the cores

Low Porosity		Medium Porosity		High Porosity	
Depth (inches)	Area fraction of voids (%)	Depth (inches)	Area fraction of voids (%)	Depth (inches)	Area fraction of voids (%)
0.004	23.1	0.004	42.4	0.004	40.9
0.008	22.8	0.007	41.7	0.008	40.2
0.012	22.5	0.011	41.2	0.011	39.4
0.015	23.5	0.014	40.6	0.015	38.7
0.019	23.3	0.018	40.1	0.019	38.1
0.023	23.1	0.021	39.6	0.023	37.5
0.027	22.9	0.025	39.2	0.026	36.8
0.031	22.9	0.029	38.1	0.030	36.2
0.035	22.8	0.032	37.7	0.034	35.8
0.039	22.6	0.036	37.4	0.038	35.3
0.043	22.5	0.039	37.1	0.042	34.8
0.046	22.4	0.043	36.8	0.045	34.5
0.050	22.3	0.046	36.5	0.049	34.0
0.054	22.1	0.050	36.2	0.053	33.6
0.058	21.9	0.054	36.0	0.057	33.1
0.062	21.7	0.057	35.8	0.061	32.7
0.066	21.5	0.061	35.5	0.064	32.4
0.070	21.4	0.064	35.3	0.068	32.1
0.073	21.2	0.068	36.0	0.072	31.9
0.077	21.0	0.071	35.8	0.076	31.6
0.081	20.9	0.075	35.6	0.079	32.3
0.085	20.8	0.078	35.3	0.083	32.3
0.089	20.5	0.082	35.2	0.087	32.1
0.093	20.3	0.086	34.9	0.091	31.9
0.097	20.1	0.089	34.8	0.095	31.7
0.101	19.9	0.093	34.6	0.098	31.6
0.104	19.7	0.096	34.4	0.102	31.4
0.108	19.5	0.100	34.2	0.106	31.4
0.112	19.3	0.103	33.9	0.110	31.2
0.116	19.2	0.107	33.8	0.113	31.1
0.120	19.1	0.111	33.5	0.117	31.0
0.124	19.0	0.114	33.4	0.121	30.9
0.128	19.0	0.118	33.2	0.125	30.8
0.131	18.8	0.121	33.0	0.129	30.7
0.135	19.8	0.125	32.7	0.132	30.8

0.139	19.7	0.128	32.4	0.136	30.8
0.143	19.6	0.132	32.2	0.140	30.9
0.147	19.5	0.136	32.0	0.144	30.9
0.151	19.6	0.139	31.7	0.148	30.8
0.155	19.5	0.143	31.5	0.151	30.8
0.159	19.4	0.146	31.3	0.155	30.8
0.162	19.5	0.150	31.1	0.159	30.8
0.166	19.4	0.153	32.0	0.163	30.8
0.170	19.6	0.157	31.9	0.166	30.8
0.174	19.7	0.161	31.8	0.170	31.9
0.178	19.7	0.164	31.7	0.174	32.0
0.182	19.7	0.168	31.6	0.178	32.1
0.186	19.7	0.171	31.5	0.182	32.1
0.189	19.6	0.175	31.4	0.185	32.2
0.193	19.5	0.178	31.5	0.189	32.2
0.197	19.5	0.182	31.3	0.193	32.2
0.201	19.4	0.186	31.2	0.197	32.2
0.205	19.2	0.189	31.1	0.200	32.3
0.209	19.2	0.193	31.0	0.204	32.2
0.213	18.9	0.196	30.9	0.208	32.3
0.217	18.7	0.200	30.9	0.212	32.3
0.220	18.6	0.203	30.8	0.216	32.3
0.224	18.3	0.207	30.7	0.219	32.4
0.228	18.0	0.210	30.5	0.223	32.3
0.232	17.7	0.214	30.3	0.227	32.3
0.236	17.4	0.218	30.2	0.231	32.3
0.240	17.2	0.221	30.1	0.235	32.3
0.244	16.8	0.225	30.1	0.238	32.3
0.247	16.5	0.228	29.9	0.242	32.3
0.251	16.3	0.232	29.8	0.246	32.2
0.255	16.1	0.235	29.7	0.250	32.1
0.259	15.9	0.239	29.6	0.253	32.0
0.263	15.8	0.243	29.5	0.257	31.8
0.267	15.7	0.246	29.5	0.261	31.7
0.271	15.6	0.250	29.5	0.265	31.6
0.275	15.6	0.253	29.5	0.269	31.5
0.278	15.6	0.257	29.5	0.272	31.4
0.282	15.4	0.260	29.5	0.276	31.4
0.286	15.3	0.264	29.5	0.280	31.2
0.290	15.2	0.268	29.4	0.284	31.0
0.294	15.3	0.271	29.2	0.287	31.0

0.298	15.3	0.275	29.1	0.291	30.8
0.302	15.4	0.278	29.0	0.295	30.7
0.305	15.4	0.282	28.9	0.299	30.7
0.309	15.5	0.285	29.9	0.303	30.5
0.313	15.6	0.289	29.8	0.306	30.4
0.317	15.7	0.293	28.4	0.310	30.5
0.321	15.7	0.296	29.5	0.314	30.5
0.325	15.7	0.300	29.3	0.318	30.7
0.329	15.6	0.303	29.1	0.322	30.8
0.333	15.5	0.307	29.0	0.325	30.9
0.336	15.4	0.310	28.8	0.329	31.0
0.340	15.4	0.314	28.4	0.333	31.1
0.344	15.3	0.318	28.0	0.337	31.1
0.348	15.2	0.321	27.6	0.340	31.3
0.352	15.1	0.325	27.2	0.344	31.3
0.356	15.1	0.328	26.8	0.348	31.5
0.360	15.2	0.332	26.5	0.352	31.7
0.363	15.2	0.335	26.2	0.356	31.8
0.367	15.3	0.339	25.8	0.359	31.8
0.371	15.5	0.343	25.4	0.363	31.8
0.375	15.6	0.346	25.2	0.367	31.9
0.379	15.8	0.350	24.8	0.371	32.0
0.383	16.0	0.353	24.5	0.374	31.9
0.387	16.2	0.357	24.1	0.378	31.9
0.391	16.3	0.360	23.9	0.382	31.9
0.394	16.5	0.364	23.8	0.386	31.8
0.398	16.6	0.367	23.5	0.390	31.8
0.402	16.8	0.371	23.3	0.393	31.9
0.406	16.9	0.375	23.0	0.397	32.0
0.410	17.2	0.378	22.9	0.401	31.9
0.414	17.4	0.382	22.8	0.405	31.8
0.418	17.6	0.385	22.6	0.409	31.8
0.421	17.7	0.389	22.4	0.412	31.7
0.425	17.9	0.392	22.3	0.416	31.7
0.429	18.2	0.396	22.3	0.420	31.8
0.433	18.4	0.400	22.4	0.424	31.7
0.437	18.7	0.403	22.4	0.427	31.8
0.441	18.9	0.407	22.3	0.431	31.8
0.445	19.1	0.410	22.1	0.435	31.8
0.449	19.4	0.414	22.0	0.439	31.8
0.452	19.4	0.417	21.8	0.443	31.8

0.456	19.6	0.421	21.8	0.446	31.6
0.460	19.6	0.425	21.7	0.450	31.5
0.464	19.8	0.428	21.8	0.454	31.5
0.468	19.8	0.432	21.8	0.458	31.4
0.472	19.8	0.435	21.6	0.461	31.1
0.476	19.8	0.439	21.5	0.465	30.8
0.479	19.7	0.442	21.5	0.469	30.7
0.483	19.6	0.446	21.3	0.473	30.5
0.487	19.7	0.450	21.2	0.477	30.4
0.491	19.8	0.453	20.9	0.480	30.3
0.495	19.7	0.457	20.8	0.484	30.3
0.499	19.7	0.460	20.7	0.488	30.3
0.503	19.8	0.464	20.6	0.492	30.3
0.507	20.0	0.467	20.6	0.496	30.4
0.510	20.1	0.471	20.6	0.499	30.4
0.514	20.3	0.475	20.5	0.503	30.5
0.518	20.4	0.478	20.5	0.507	30.5
0.522	20.5	0.482	20.5	0.511	30.4
0.526	20.6	0.485	20.5	0.514	30.5
0.530	20.6	0.489	20.6	0.518	30.5
0.534	20.8	0.492	20.6	0.522	30.6
0.537	20.6	0.496	20.6	0.526	30.7
0.541	20.6	0.499	20.8	0.530	30.6
0.545	20.4	0.503	21.1	0.533	30.6
0.549	20.3	0.507	21.3	0.537	30.5
0.553	20.2	0.510	21.5	0.541	30.7
0.557	20.2	0.514	21.5	0.545	30.7
0.561	20.1	0.517	21.6	0.548	30.7
0.565	20.0	0.521	21.7	0.552	30.7
0.568	20.0	0.524	21.7	0.556	30.7
0.572	20.0	0.528	21.7	0.560	30.6
0.576	18.6	0.532	21.7	0.564	30.6
0.580	18.6	0.535	21.7	0.567	30.6
0.584	18.6	0.539	21.6	0.571	30.5
0.588	18.7	0.542	21.6	0.575	30.5
0.592	18.8	0.546	21.6	0.579	30.6
0.595	18.7	0.549	21.6	0.583	30.6
0.599	18.8	0.553	21.6	0.586	30.6
0.603	18.9	0.557	21.6	0.590	30.6
0.607	18.9	0.560	20.5	0.594	30.6
0.611	18.9	0.564	21.5	0.598	30.6

0.615	18.8	0.567	21.6	0.601	30.7
0.619	19.0	0.571	21.5	0.605	30.8
0.623	19.0	0.574	21.5	0.609	30.8
0.626	19.3	0.578	21.6	0.613	30.9
0.630	19.4	0.582	21.7	0.617	30.9
0.634	19.4	0.585	21.8	0.620	31.0
0.638	19.6	0.589	22.0	0.624	31.0
0.642	19.7	0.592	22.0	0.628	31.2
0.646	19.9	0.596	22.2	0.632	31.3
0.650	20.0	0.599	22.4	0.635	31.4
0.653	20.2	0.603	22.6	0.639	31.6
0.657	20.2	0.607	22.9	0.643	31.8
0.661	20.3	0.610	23.2	0.647	32.0
0.665	20.4	0.614	23.4	0.651	32.2
0.669	20.5	0.617	23.9	0.654	32.6
0.673	20.5	0.621	24.1	0.658	32.9
0.677	20.6	0.624	24.6	0.662	33.2
0.681	20.8	0.628	24.9	0.666	33.5
0.684	20.9	0.631	25.1	0.670	33.7
0.688	20.7	0.635	25.2	0.673	34.0
0.692	20.9	0.639	25.4	0.677	34.2
0.696	20.9	0.642	25.6	0.681	34.3
0.700	21.0	0.646	25.7	0.685	34.6
0.704	21.0	0.649	25.7	0.688	34.8
0.708	21.0	0.653	25.7	0.692	35.1
0.711	21.0	0.656	25.7	0.696	35.3
0.715	21.0	0.660	25.8	0.700	35.4
0.719	21.0	0.664	26.0	0.704	35.6
0.723	21.0	0.667	26.1	0.707	35.8
0.727	21.0	0.671	26.1	0.711	34.8
0.731	20.9	0.674	26.1	0.715	36.1
0.735	20.9	0.678	26.2	0.719	34.9
0.739	20.9	0.681	26.2	0.722	35.0
0.742	20.9	0.685	26.1	0.726	35.1
0.746	21.0	0.689	26.0	0.730	36.3
0.750	21.0	0.692	26.0	0.734	36.3
0.754	21.1	0.696	26.0	0.738	36.1
0.758	21.0	0.699	25.9	0.741	35.9
0.762	21.0	0.703	24.3	0.745	35.6
0.766	20.9	0.706	24.3	0.749	35.4
0.769	20.8	0.710	24.2	0.753	35.2

0.773	20.8	0.714	24.1	0.757	34.9
0.777	20.7	0.717	25.5	0.760	34.7
0.781	20.9	0.721	25.7	0.764	34.5
0.785	20.7	0.724	25.5	0.768	34.2
0.789	20.6	0.728	23.9	0.772	33.9
0.793	20.6	0.731	23.9	0.775	33.5
0.797	20.8	0.735	23.8	0.779	33.2
0.800	20.6	0.739	23.6	0.783	33.0
0.804	20.6	0.742	23.5	0.787	32.7
0.808	20.6	0.746	23.3	0.791	32.3
0.812	20.6	0.749	23.4	0.794	31.9
0.816	20.4	0.753	23.2	0.798	31.5
0.820	20.4	0.756	23.1	0.802	31.2
0.824	20.4	0.760	22.9	0.806	31.0
0.827	20.5	0.764	22.7	0.809	30.6
0.831	20.6	0.767	22.6	0.813	30.3
0.835	20.6	0.771	22.6	0.817	30.1
0.839	20.5	0.774	22.5	0.821	29.7
0.843	20.5	0.778	22.4	0.825	29.4
0.847	20.6	0.781	22.2	0.828	29.2
0.851	20.7	0.785	22.0	0.832	27.8
0.855	20.7	0.788	21.9	0.836	27.7
0.858	20.6	0.792	21.8	0.840	27.7
0.862	20.6	0.796	21.8	0.843	27.6
0.866	19.4	0.799	21.9	0.847	27.7
0.870	19.4	0.803	22.0	0.851	27.6
0.874	19.5	0.806	22.0	0.855	27.6
0.878	19.5	0.810	22.4	0.859	27.6
0.882	19.5	0.813	22.7	0.862	27.8
0.885	19.7	0.817	22.9	0.866	27.9
0.889	19.7	0.821	22.9	0.870	28.0
0.893	19.8	0.824	23.0	0.874	28.1
0.897	19.8	0.828	23.1	0.878	28.3
0.901	19.9	0.831	23.2	0.881	28.3
0.905	20.0	0.835	23.3	0.885	28.4
0.909	20.2	0.838	23.3	0.889	28.6
0.913	20.2	0.842	23.4	0.893	28.8
0.916	20.1	0.846	23.3	0.896	28.9
0.920	21.6	0.849	23.4	0.900	28.9
0.924	20.2	0.853	23.5	0.904	29.0
0.928	20.2	0.856	23.4	0.908	29.2

0.932	20.2	0.860	23.5	0.912	29.4
0.936	20.2	0.863	23.5	0.915	29.6
0.940	20.2	0.867	23.7	0.919	29.7
0.944	20.1	0.871	23.8	0.923	29.8
0.947	20.2	0.874	24.0	0.927	30.0
0.951	20.1	0.878	23.9	0.930	30.2
0.955	20.0	0.881	24.0	0.934	30.4
0.959	19.8	0.885	23.9	0.938	30.5
0.963	19.7	0.888	23.8	0.942	30.7
0.967	19.6	0.892	23.8	0.946	30.9
0.971	19.4	0.896	23.8	0.949	31.0
0.974	19.4	0.899	23.8	0.953	31.2
0.978	19.3	0.903	23.9	0.957	31.4
0.982	19.4	0.906	24.2	0.961	31.6
0.986	19.2	0.910	24.4	0.965	31.9
0.990	19.2	0.913	24.7	0.968	32.2
0.994	19.1	0.917	24.9	0.972	32.4
0.998	19.0	0.920	24.7	0.976	32.6
1.002	18.9	0.924	24.6	0.980	32.8
1.005	18.8	0.928	24.8	0.983	33.0
1.009	18.6	0.931	24.8	0.987	33.3
1.013	18.3	0.935	24.8	0.991	33.6
1.017	18.2	0.938	24.7	0.995	33.7
1.021	19.5	0.942	24.7	0.999	34.0
1.025	19.2	0.945	24.7	1.002	34.3
1.029	19.2	0.949	24.8	1.006	34.3
1.032	19.1	0.953	24.7	1.010	34.2
1.036	18.9	0.956	24.7	1.014	34.2
1.040	18.9	0.960	24.7	1.017	34.1
1.044	18.9	0.963	24.4	1.021	34.1
1.048	18.8	0.967	24.4	1.025	34.0
1.052	18.7	0.970	24.5	1.029	34.0
1.056	18.8	0.974	24.4	1.033	33.9
1.060	18.7	0.978	24.2	1.036	33.7
1.063	18.7	0.981	24.2	1.040	33.7
1.067	18.7	0.985	24.1	1.044	33.7
1.071	18.9	0.988	24.2	1.048	33.9
1.075	18.9	0.992	24.2	1.052	33.9
1.079	18.8	0.995	24.1	1.055	34.0
1.083	18.7	0.999	24.1	1.059	34.1
1.087	18.9	1.003	24.0	1.063	34.3

1.090	18.9	1.006	24.1	1.067	34.4
1.094	18.9	1.010	24.1	1.070	34.5
1.098	18.9	1.013	24.0	1.074	34.5
1.102	18.9	1.017	23.8	1.078	34.6
1.106	17.6	1.020	23.6	1.082	34.8
1.110	17.7	1.024	23.4	1.086	34.7
1.114	19.1	1.028	23.4	1.089	34.8
1.118	17.9	1.031	23.1	1.093	34.9
1.121	19.3	1.035	22.8	1.097	35.1
1.125	19.3	1.038	22.7	1.101	35.2
1.129	19.3	1.042	22.6	1.104	35.3
1.133	18.1	1.045	22.4	1.108	35.3
1.137	18.1	1.049	22.2	1.112	35.4
1.141	18.0	1.052	22.1	1.116	35.4
1.145	19.3	1.056	22.1	1.120	35.3
1.148	19.3	1.060	22.0	1.123	35.1
1.152	19.5	1.063	21.9	1.127	35.2
1.156	19.5	1.067	21.9	1.131	35.0
1.160	19.5	1.070	21.6	1.135	35.0
1.164	19.3	1.074	21.4	1.139	34.9
1.168	19.3	1.077	21.3	1.142	34.8
1.172	19.2	1.081	21.0	1.146	34.8
1.176	19.1	1.085	20.8	1.150	34.8
1.179	18.8	1.088	20.4	1.154	34.7
1.183	18.6	1.092	20.0	1.157	34.7
1.187	18.2	1.095	19.8	1.161	34.7
1.191	18.0	1.099	19.3	1.165	34.7
1.195	17.8	1.102	18.9	1.169	34.8
1.199	17.7	1.106	18.5	1.173	34.7
1.203	17.3	1.110	18.3	1.176	34.6
1.206	17.3	1.113	18.3	1.180	34.6
1.210	17.2	1.117	18.3	1.184	34.4
1.214	17.0	1.120	18.3	1.188	34.3
1.218	16.8	1.124	18.4	1.191	34.2
1.222	16.8	1.127	18.3	1.195	34.0
1.226	16.7	1.131	18.3	1.199	33.8
1.230	16.7	1.135	18.3	1.203	33.6
1.234	16.7	1.138	18.3	1.207	33.5
1.237	16.7	1.142	18.3	1.210	33.5
1.241	16.8	1.145	18.4	1.214	33.3
1.245	16.8	1.149	18.3	1.218	33.3

1.249	16.6	1.152	18.2	1.222	32.9
1.253	16.5	1.156	18.0	1.226	32.6
1.257	16.3	1.160	18.0	1.229	32.3
1.261	16.6	1.163	17.9	1.233	31.9
1.264	16.5	1.167	18.1	1.237	31.5
1.268	16.4	1.170	18.2	1.241	31.2
1.272	16.4	1.174	18.3	1.244	31.0
1.276	16.3	1.177	18.3	1.248	30.8
1.280	16.2	1.181	18.5	1.252	30.4
1.284	16.1	1.185	18.7	1.256	30.0
1.288	16.0	1.188	18.8	1.260	29.7
1.292	16.1	1.192	19.0	1.263	29.2
1.295	15.9	1.195	19.2	1.267	28.8
1.299	15.9	1.199	19.6	1.271	28.3
1.303	15.8	1.202	19.8	1.275	27.8
1.307	15.7	1.206	20.2	1.278	27.4
1.311	15.8	1.209	20.7	1.282	27.1
1.315	15.6	1.213	20.9	1.286	26.8
1.319	15.6	1.217	21.2	1.290	26.6
1.322	15.2	1.220	21.7	1.294	26.4
1.326	15.3	1.224	22.1	1.297	26.2
1.330	15.1	1.227	22.6	1.301	26.2
1.334	14.8	1.231	22.9	1.305	25.9
1.338	14.6	1.234	23.4	1.309	25.7
1.342	14.6	1.238	22.1	1.313	25.6
1.346	14.3	1.242	22.3	1.316	25.7
1.350	14.2	1.245	22.5	1.320	25.6
1.353	14.1	1.249	22.9	1.324	25.6
1.357	14.1	1.252	23.1	1.328	25.4
1.361	14.1	1.256	23.2	1.331	25.4
1.365	13.9	1.259	23.2	1.335	25.2
1.369	14.0	1.263	23.3	1.339	25.3
1.373	14.1	1.267	23.5	1.343	25.3
1.377	14.3	1.270	23.6	1.347	25.3
1.380	14.2	1.274	23.6	1.350	25.4
1.384	14.4	1.277	23.6	1.354	25.5
1.388	14.7	1.281	23.6	1.358	25.5
1.392	14.8	1.284	23.5	1.362	25.5
1.396	15.1	1.288	23.4	1.365	25.6
1.400	15.2	1.292	23.2	1.369	25.5
1.404	15.2	1.295	23.0	1.373	25.6

1.408	15.3	1.299	22.7	1.377	25.5
1.411	15.5	1.302	22.8	1.381	25.7
1.415	15.7	1.306	22.7	1.384	25.6
1.419	15.8	1.309	22.6	1.388	25.8
1.423	15.9	1.313	22.3	1.392	25.8
1.427	16.1	1.317	22.1	1.396	25.8
1.431	16.3	1.320	22.1	1.400	26.0
1.435	16.7	1.324	22.2	1.403	26.2
1.438	16.8	1.327	22.0	1.407	26.4
1.442	17.0	1.331	22.0	1.411	26.4
1.446	17.3	1.334	21.9	1.415	26.5
1.450	17.4	1.338	21.8	1.418	26.6
1.454	17.4	1.341	21.7	1.422	26.8
1.458	15.7	1.345	21.6	1.426	26.9
1.462	15.8	1.349	21.5	1.430	26.9
1.466	15.8	1.352	21.4	1.434	26.8
1.469	15.8	1.356	21.4	1.437	26.9
1.473	15.7	1.359	21.3	1.441	27.0
1.477	15.7	1.363	22.9	1.445	27.1
1.481	15.7	1.366	22.6	1.449	27.1
1.485	15.8	1.370	22.3	1.452	27.1
1.489	15.8	1.374	22.1	1.456	27.1
1.493	15.9	1.377	22.1	1.460	27.0
1.496	15.9	1.381	21.8	1.464	27.0
1.500	16.0	1.384	21.4	1.468	26.8
1.504	15.9	1.388	21.1	1.471	26.5
1.508	15.9	1.391	20.9	1.475	26.2
1.512	15.8	1.395	20.9	1.479	26.0
1.516	17.6	1.399	20.7	1.483	25.7
1.520	15.8	1.402	20.5	1.487	25.4
1.524	15.8	1.406	20.3	1.490	25.3
1.527	15.8	1.409	20.2	1.494	25.2
1.531	15.9	1.413	20.1	1.498	25.0
1.535	16.0	1.416	20.1	1.502	24.8
1.539	16.2	1.420	20.1	1.505	24.6
1.543	16.4	1.424	19.7	1.509	24.3
1.547	16.5	1.427	19.6	1.513	24.0
1.551	16.7	1.431	19.3	1.517	23.7
1.554	16.7	1.434	19.2	1.521	23.5
1.558	16.9	1.438	19.1	1.524	23.4
1.562	17.2	1.441	18.9	1.528	23.4

1.566	17.4	1.445	18.7	1.532	23.3
1.570	17.6	1.449	18.4	1.536	23.2
1.574	17.8	1.452	18.1	1.539	23.1
1.578	18.1	1.456	18.0	1.543	22.9
1.582	18.4	1.459	17.9	1.547	22.8
1.585	18.4	1.463	17.5	1.551	22.6
1.589	18.5	1.466	17.5	1.555	24.0
1.593	18.6	1.470	17.5	1.558	22.5
1.597	18.4	1.473	17.3	1.562	22.3
1.601	18.2	1.477	17.2	1.566	22.3
1.605	18.2	1.481	17.2	1.570	22.4
1.609	18.1	1.484	17.2	1.574	22.4
1.612	18.0	1.488	17.1	1.577	22.5
1.616	18.0	1.491	16.9	1.581	22.5
1.620	17.9	1.495	17.1	1.585	22.8
1.624	17.7	1.498	17.2	1.589	23.0
1.628	17.6	1.502	17.5	1.592	23.3
1.632	17.4	1.506	17.7	1.596	23.4
1.636	17.1	1.509	17.9	1.600	23.6
1.640	17.0	1.513	18.2	1.604	23.9
1.643	16.7	1.516	18.4	1.608	25.6
1.647	16.4	1.520	18.7	1.611	25.8
1.651	16.3	1.523	18.9	1.615	25.9
1.655	16.0	1.527	19.4	1.619	26.4
1.659	15.8	1.531	19.8	1.623	26.6
1.663	15.7	1.534	20.1	1.626	25.1
1.667	15.4	1.538	20.3	1.630	25.2
1.670	15.1	1.541	20.6	1.634	25.3
1.674	15.0	1.545	21.0	1.638	25.5
1.678	14.8	1.548	21.5	1.642	25.8
1.682	14.5	1.552	22.1	1.645	26.0
1.686	14.2	1.556	22.3	1.649	26.2
1.690	14.0	1.559	22.7	1.653	26.5
1.694	15.7	1.563	23.1	1.657	26.8
1.698	15.6	1.566	23.4	1.661	27.0
1.701	15.3	1.570	23.7	1.664	27.1
1.705	15.1	1.573	24.0	1.668	27.5
1.709	15.0	1.577	24.3	1.672	27.7
1.713	14.8	1.581	24.7	1.676	27.9
1.717	14.8	1.584	25.0	1.679	28.1
1.721	14.8	1.588	23.0	1.683	28.5

A-11

1.725	14.4	1.591	23.2	1.687	28.7
1.728	14.3	1.595	23.6	1.691	28.8
1.732	14.1	1.598	23.8	1.695	28.8
1.736	14.2	1.602	24.0	1.698	28.8
1.740	14.2	1.606	24.1	1.702	28.7
1.744	14.1	1.609	24.0	1.706	28.6
1.748	12.2	1.613	24.1	1.710	28.7
1.752	12.0	1.616	23.9	1.713	28.8
1.756	12.0	1.620	24.1	1.717	28.9
1.759	11.9	1.623	24.0	1.721	28.7
1.763	12.0	1.627	23.9	1.725	28.6
1.767	12.1	1.630	23.9	1.729	28.7
1.771	12.2	1.634	23.9	1.732	28.7
1.775	12.2	1.638	25.7	1.736	28.6
1.779	12.3	1.641	25.7	1.740	28.5
1.783	12.4	1.645	25.7	1.744	28.4
1.786	12.4	1.648	25.6	1.748	28.3
1.790	12.6	1.652	25.5	1.751	28.2
1.794	12.6	1.655	25.3	1.755	28.3
1.798	12.8	1.659	25.3	1.759	28.1
1.802	12.9	1.663	25.2	1.763	28.0
1.806	12.9	1.666	24.9	1.766	28.2
1.810	12.9	1.670	24.6	1.770	28.3
1.814	13.0	1.673	24.3	1.774	28.2
1.817	13.1	1.677	24.1	1.778	28.3
1.821	13.1	1.680	24.1	1.782	28.4
1.825	13.0	1.684	24.0	1.785	28.6
1.829	13.0	1.688	24.0	1.789	28.8
1.833	14.9	1.691	23.8	1.793	29.0
1.837	15.1	1.695	23.7	1.797	29.1
1.841	15.1	1.698	23.5	1.800	29.3
1.844	15.0	1.702	23.2	1.804	29.3
1.848	15.2	1.705	20.7	1.808	29.4
1.852	15.2	1.709	20.6	1.812	29.5
1.856	15.1	1.713	20.4	1.816	29.6
1.860	15.3	1.716	22.7	1.819	29.6
1.864	15.5	1.720	22.7	1.823	29.7
1.868	15.6	1.723	20.5	1.827	29.7
1.872	15.3	1.727	20.3	1.831	29.6
1.875	15.0	1.730	20.4	1.835	29.3
1.879	15.3	1.734	20.4	1.838	29.3

1.883	15.4	1.738	20.4	1.842	29.1
1.887	15.5	1.741	20.7	1.846	28.9
1.891	15.3	1.745	20.6	1.850	28.8
1.895	15.3	1.748	20.6	1.853	28.7
1.899	15.4	1.752	20.6	1.857	28.5
1.902	15.4	1.755	20.6	1.861	28.4
1.906	15.2	1.759	20.5	1.865	28.3
1.910	15.0	1.762	22.3	1.869	28.2
1.914	14.9	1.766	22.0	1.872	28.0
1.918	15.1	1.770	22.0	1.876	27.9
1.922	14.9	1.773	22.0	1.880	28.1
1.926	14.6	1.777	21.7	1.884	28.2
1.930	14.5	1.780	21.4	1.887	28.1
1.933	14.4	1.784	21.6	1.891	28.3
1.937	14.4	1.787	21.4	1.895	28.4
1.941	14.3	1.791	21.2	1.899	28.3
1.945	14.4	1.795	21.1	1.903	28.3
1.949	14.6	1.798	21.3	1.906	28.4
1.953	14.3	1.802	21.3	1.910	28.5
1.957	14.4	1.805	21.4	1.914	28.4
1.960	14.5	1.809	21.5	1.918	28.3
1.964	12.7	1.812	21.3	1.922	28.3
1.968	12.8	1.816	21.3	1.925	28.1
1.972	12.9	1.820	21.3	1.929	28.1
1.976	12.9	1.823	21.2	1.933	28.1
1.980	12.8	1.827	21.0	1.937	28.0
1.984	12.7	1.830	21.0	1.940	28.1
1.988	12.7	1.834	21.0	1.944	28.0
1.991	12.9	1.837	21.0	1.948	28.2
1.995	12.9	1.841	21.3	1.952	28.3
1.999	12.9	1.845	21.2	1.956	28.6
2.003	12.9	1.848	21.0	1.959	28.7
2.007	13.1	1.852	21.1	1.963	28.8
2.011	13.3	1.855	21.1	1.967	29.0
2.015	13.4	1.859	21.2	1.971	29.0
2.018	13.3	1.862	21.1	1.974	29.2
2.022	13.2	1.866	21.1	1.978	29.4
2.026	13.1	1.870	21.2	1.982	29.5
2.030	14.6	1.873	21.0	1.986	29.6
2.034	14.4	1.877	21.1	1.990	29.6
2.038	14.5	1.880	21.1	1.993	29.7

2.042	14.6	1.884	21.0	1.997	29.7
2.046	14.2	1.887	21.0	2.001	29.6
2.049	14.1	1.891	21.1	2.005	29.5
2.053	14.2	1.894	21.1	2.009	29.4
2.057	14.1	1.898	21.1	2.012	29.4
2.061	13.9	1.902	21.4	2.016	29.1
2.065	13.8	1.905	21.4	2.020	29.0
2.069	13.6	1.909	21.4	2.024	28.8
2.073	13.6	1.912	21.7	2.027	28.7
2.076	13.7	1.916	21.7	2.031	28.3
2.080	13.6	1.919	21.5	2.035	28.1
2.084	13.4	1.923	21.4	2.039	27.8
2.088	13.3	1.927	21.6	2.043	27.6
2.092	13.2	1.930	21.8	2.046	27.4
2.096	15.5	1.934	21.7	2.050	27.1
2.100	15.5	1.937	21.5	2.054	26.8
2.104	12.4	1.941	21.1	2.058	26.6
2.107	12.2	1.944	20.9	2.061	26.4
2.111	12.1	1.948	21.1	2.065	26.1
2.115	14.5	1.952	21.3	2.069	26.0
2.119	14.6	1.955	21.1	2.073	25.9
2.123	11.9	1.959	21.0	2.077	25.8
2.127	11.4	1.962	21.1	2.080	25.8
2.131	13.8	1.966	21.2	2.084	25.9
2.134	13.9	1.969	21.2	2.088	26.0
2.138	14.0	1.973	21.2	2.092	26.2
2.142	11.6	1.977	21.1	2.096	26.2
2.146	14.0	1.980	21.0	2.099	26.1
2.150	11.6	1.984	20.6	2.103	26.2
2.154	14.2	1.987	20.3	2.107	26.1
2.158	12.0	1.991	20.1	2.111	26.1
2.162	12.1	1.994	20.1	2.114	26.1
2.165	11.9	1.998	20.0	2.118	26.1
2.169	12.0	2.002	19.8	2.122	26.1
2.173	14.3	2.005	19.6	2.126	26.0
2.177	14.2	2.009	19.7	2.130	26.0
2.181	14.1	2.012	19.6	2.133	25.8
2.185	14.0	2.016	19.3	2.137	25.8
2.189	13.9	2.019	18.8	2.141	25.7
2.192	14.0	2.023	18.7	2.145	25.6
2.196	13.6	2.027	18.4	2.148	25.5

2.200	11.2	2.030	18.5	2.152	25.6
2.204	13.5	2.034	18.3	2.156	25.6
2.208	13.6	2.037	18.3	2.160	25.7
2.212	13.4	2.041	18.2	2.164	25.6
2.216	13.3	2.044	18.1	2.167	25.6
2.220	13.2	2.048	18.1	2.171	25.5
2.223	13.1	2.051	18.0	2.175	25.6
2.227	12.7	2.055	17.9	2.179	25.5
2.231	12.6	2.059	18.0	2.183	25.4
2.235	12.5	2.062	18.1	2.186	25.4
2.239	12.2	2.066	18.3	2.190	26.8
2.243	12.3	2.069	18.1	2.194	26.8
2.247	11.9	2.073	18.0	2.198	26.9
2.250	11.8	2.076	17.9	2.201	26.9
2.254	11.6	2.080	17.9	2.205	26.8
2.258	11.5	2.084	17.8	2.209	26.8
2.262	11.4	2.087	17.5	2.213	26.8
2.266	11.6	2.091	17.2	2.217	26.8
2.270	11.7	2.094	17.3	2.220	26.7
2.274	11.7	2.098	17.1	2.224	26.7
2.278	11.5	2.101	16.8	2.228	26.9
2.281	11.5	2.105	16.7	2.232	26.9
2.285	11.7	2.109	16.7	2.235	26.9
2.289	12.0	2.112	16.6	2.239	26.9
2.293	12.0	2.116	16.4	2.243	26.7
2.297	11.8	2.119	16.2	2.247	26.7
2.301	11.8	2.123	16.3	2.251	26.7
2.305	11.7	2.126	16.2	2.254	26.6
2.308	11.8	2.130	16.1	2.258	26.6
2.312	11.6	2.134	15.8	2.262	26.5
2.316	11.8	2.137	15.8	2.266	26.6
2.320	12.0	2.141	15.8	2.270	26.7
2.324	12.0	2.144	15.6	2.273	26.7
2.328	12.1	2.148	15.6	2.277	26.6
2.332	12.2	2.151	15.7	2.281	26.6
2.336	12.2	2.155	15.7	2.285	26.6
2.339	12.2	2.159	15.7	2.288	26.7
2.343	12.4	2.162	15.7	2.292	26.7
2.347	12.4	2.166	15.9	2.296	26.6
2.351	12.5	2.169	16.1	2.300	26.8
2.355	12.4	2.173	16.0	2.304	26.9

2.359	12.3	2.176	16.0	2.307	26.9
2.363	12.3	2.180	16.3	2.311	27.0
2.366	12.2	2.183	16.5	2.315	27.1
2.370	12.0	2.187	16.7	2.319	27.0
2.374	11.9	2.191	17.0	2.322	26.9
2.378	11.8	2.194	17.2	2.326	26.8
2.382	12.0	2.198	17.5	2.330	26.8
2.386	11.9	2.201	17.7	2.334	26.8
2.390	11.9	2.205	17.8	2.338	26.8
2.394	11.8	2.208	17.9	2.341	26.8
2.397	11.8	2.212	18.0	2.345	26.9
2.401	11.6	2.216	18.2	2.349	27.0
2.405	11.3	2.219	18.3	2.353	27.2
2.409	11.4	2.223	18.2	2.357	27.3
2.413	11.4	2.226	18.2	2.360	27.3
2.417	11.3	2.230	18.2	2.364	27.4
2.421	11.4	2.233	18.0	2.368	27.3
2.424	11.1	2.237	17.8	2.372	27.1
2.428	11.0	2.241	17.6	2.375	26.9
2.432	10.6	2.244	17.7	2.379	26.7
2.436	10.5	2.248	17.5	2.383	26.6
2.440	10.5	2.251	19.6	2.387	26.5
2.444	10.3	2.255	19.0	2.391	26.3
2.448	10.1	2.258	16.6	2.394	26.2
2.452	10.0	2.262	18.9	2.398	26.1
2.455	9.8	2.266	18.5	2.402	26.0
2.459	9.8	2.269	18.2	2.406	26.0
2.463	10.0	2.273	18.0	2.409	26.0
2.467	9.9	2.276	17.9	2.413	25.9
2.471	9.5	2.280	17.7	2.417	25.9
2.475	9.6	2.283	17.7	2.421	25.7
2.479	9.4	2.287	17.6	2.425	25.5
2.482	9.3	2.291	17.5	2.428	25.2
2.486	9.3	2.294	17.1	2.432	24.9
2.490	9.1	2.298	17.0	2.436	24.7
2.494	11.7	2.301	17.0	2.440	24.6
2.498	11.8	2.305	16.7	2.443	24.4
2.502	11.6	2.308	16.2	2.447	24.2
2.506	11.5	2.312	16.1	2.451	24.2
2.510	11.5	2.315	16.2	2.455	24.0
2.513	11.3	2.319	15.8	2.459	23.8

A-16

2.517	11.0	2.323	15.6	2.462	23.6
2.521	11.1	2.326	15.4	2.466	23.6
2.525	11.1	2.330	15.0	2.470	23.4
2.529	11.1	2.333	14.7	2.474	23.5
2.533	8.6	2.337	14.3	2.478	23.4
2.537	11.0	2.340	14.2	2.481	23.3
2.540	11.3	2.344	14.1	2.485	23.0
2.544	10.9	2.348	13.9	2.489	22.8
2.548	11.3	2.351	13.7	2.493	22.7
2.552	9.1	2.355	13.4	2.496	22.5
2.556	9.1	2.358	13.2	2.500	22.3
2.560	9.1	2.362	13.2	2.504	23.4
2.564	9.3	2.365	12.9	2.508	23.3
2.568	9.5	2.369	12.8	2.512	23.1
2.571	9.6	2.373	13.0	2.515	22.9
2.575	12.1	2.376	13.1	2.519	22.8
2.579	9.7	2.380	13.0	2.523	22.7
2.583	9.8	2.383	12.9	2.527	22.5
2.587	9.7	2.387	12.9	2.530	22.3
2.591	9.9	2.390	12.9	2.534	22.0
2.595	10.1	2.394	13.1	2.538	21.7
2.598	10.1	2.398	13.2	2.542	21.5
2.602	10.2	2.401	13.1	2.546	21.4
2.606	10.4	2.405	13.0	2.549	21.3
2.610	10.4	2.408	13.1	2.553	21.2
2.614	10.7	2.412	12.9	2.557	21.0
2.618	10.8	2.415	13.1	2.561	20.7
2.622	10.9	2.419	13.0	2.565	20.5
2.626	11.0	2.423	13.0	2.568	20.5
2.629	11.2	2.426	13.0	2.572	20.4
2.633	11.3	2.430	13.0	2.576	20.2
2.637	11.2	2.433	12.8	2.580	20.1
2.641	11.1	2.437	12.9	2.583	20.1
2.645	11.2	2.440	13.0	2.587	20.1
2.649	11.3	2.444	15.0	2.591	20.0
2.653	11.3	2.448	14.8	2.595	20.1
2.656	11.3	2.451	14.8	2.599	20.1
2.660	11.2	2.455	14.7	2.602	20.1
2.664	11.1	2.458	14.6	2.606	20.0
2.668	11.0	2.462	14.4	2.610	20.0
2.672	11.0	2.465	14.4	2.614	19.9

A-17

2.676	10.9	2.469	14.0	2.617	19.9
2.680	10.8	2.472	14.2	2.621	19.9
2.684	10.7	2.476	14.2	2.625	19.8
2.687	10.5	2.480	14.2	2.629	19.7
2.691	10.5	2.483	14.2	2.633	19.7
2.695	10.5	2.487	14.0	2.636	19.8
2.699	10.4	2.490	14.1	2.640	19.8
2.703	10.1	2.494	13.9	2.644	19.8
2.707	10.0	2.497	13.6	2.648	20.0
2.711	9.9	2.501	13.5	2.652	20.1
2.715	9.8	2.505	13.4	2.655	20.2
2.718	11.4	2.508	13.4	2.659	20.3
2.722	11.1	2.512	13.2	2.663	20.5
2.726	9.4	2.515	13.0	2.667	20.7
2.730	10.8	2.519	13.2	2.670	20.6
2.734	10.3	2.522	13.3	2.674	20.6
2.738	10.2	2.526	13.1	2.678	20.6
2.742	9.9	2.530	13.2	2.682	20.5
2.745	9.9	2.533	13.2	2.686	20.5
2.749	9.6	2.537	12.9	2.689	20.5
2.753	9.5	2.540	12.8	2.693	20.5
2.757	9.3	2.544	12.7	2.697	20.5
2.761	9.1	2.547	12.8	2.701	20.6
2.765	8.8	2.551	12.9	2.704	20.7
2.769	8.6	2.555	12.7	2.708	20.8
2.773	8.5	2.558	12.6	2.712	20.9
2.776	8.5	2.562	12.4	2.716	20.9
2.780	8.3	2.565	12.4	2.720	21.1
2.784	8.1	2.569	10.8	2.723	21.1
2.788	8.1	2.572	10.9	2.727	21.1
2.792	8.0	2.576	11.1	2.731	21.1
2.796	8.0	2.580	10.9	2.735	21.1
2.800	8.0	2.583	10.9	2.739	21.2
2.803	8.1	2.587	12.6	2.742	21.2
2.807	8.0	2.590	12.6	2.746	20.9
2.811	8.0	2.594	11.1	2.750	20.9
2.815	7.9	2.597	11.2	2.754	20.8
2.819	8.2	2.601	11.1	2.757	20.6
2.823	8.1	2.604	11.0	2.761	20.4
2.827	8.2	2.608	10.9	2.765	20.3
2.831	8.3	2.612	10.8	2.769	20.0

2.834	8.2	2.615	10.7	2.773	19.7
2.838	8.2	2.619	10.5	2.776	19.6
2.842	8.3	2.622	10.5	2.780	19.3
2.846	8.3	2.626	10.4	2.784	19.1
2.850	8.0	2.629	10.4	2.788	18.9
2.854	8.0	2.633	10.1	2.791	18.7
2.858	7.8	2.637	10.0	2.795	18.5
2.861	7.8	2.640	9.9	2.799	18.4
2.865	7.8	2.644	9.9	2.803	18.3
2.869	7.9	2.647	9.7	2.807	18.2
2.873	7.7	2.651	9.6	2.810	18.2
2.877	7.7	2.654	9.5	2.814	18.1
2.881	7.5	2.658	9.5	2.818	18.1
2.885	7.2	2.662	9.3	2.822	18.2
2.889	7.0	2.665	9.3	2.826	18.3
2.892	7.0	2.669	9.2	2.829	18.4
2.896	6.7	2.672	9.2	2.833	18.6
2.900	6.6	2.676	9.1	2.837	18.6
2.904	8.3	2.679	9.1	2.841	18.8
2.908	8.2	2.683	9.0	2.844	18.9
2.912	8.1	2.687	8.8	2.848	19.1
2.916	8.1	2.690	8.6	2.852	19.3
2.919	7.9	2.694	8.6	2.856	19.5
2.923	6.2	2.697	8.6	2.860	19.7
2.927	7.9	2.701	8.5	2.863	19.8
2.931	6.3	2.704	8.5	2.867	20.0
2.935	6.2	2.708	8.5	2.871	20.2
2.939	6.3	2.712	8.6	2.875	20.4
2.943	6.3	2.715	8.7	2.878	20.5
2.947	6.3	2.719	9.8	2.882	20.7
2.950	6.2	2.722	8.6	2.886	20.9
2.954	6.2	2.726	8.7	2.890	21.1
2.958	6.4	2.729	8.8	2.894	21.3
2.962	6.3	2.733	8.8	2.897	21.6
2.966	6.3	2.736	8.9	2.901	21.8
2.970	6.4	2.740	8.9	2.905	21.9
2.974	6.2	2.744	9.1	2.909	22.1
2.977	6.2	2.747	9.1	2.913	22.4
2.981	6.2	2.751	9.2	2.916	22.6
2.985	6.2	2.754	9.4	2.920	22.9
2.989	6.1	2.758	9.4	2.924	23.1

2.993	6.2	2.761	9.5	2.928	23.2
2.997	6.3	2.765	9.6	2.931	23.4
3.001	6.4	2.769	9.6	2.935	23.7
3.005	6.4	2.772	9.8	2.939	23.9
3.008	6.5	2.776	9.8	2.943	24.1
3.012	6.4	2.779	10.8	2.947	24.2
3.016	6.5	2.783	10.9	2.950	24.5
3.020	6.3	2.786	11.0	2.954	24.6
3.024	6.5	2.790	11.1	2.958	24.6
3.028	6.5	2.794	10.9	2.962	24.9
3.032	6.4	2.797	10.8	2.965	25.1
3.035	6.5	2.801	10.8	2.969	25.2
3.039	6.4	2.804	10.8	2.973	25.5
3.043	6.4	2.808	10.7	2.977	25.7
3.047	6.3	2.811	10.6	2.981	25.7
3.051	6.3	2.815	10.5	2.984	25.7
3.055	7.6	2.819	10.3	2.988	26.0
3.059	7.5	2.822	10.3	2.992	26.1
3.063	7.6	2.826	10.3	2.996	26.1
3.066	7.4	2.829	10.1	3.000	26.2
3.070	7.4	2.833	10.0	3.003	26.3
3.074	7.4	2.836	9.7	3.007	26.2
3.078	7.5	2.840	9.6	3.011	26.1
3.082	7.6	2.844	9.6	3.015	26.1
3.086	7.7	2.847	9.6	3.018	25.9
3.090	7.7	2.851	9.7	3.022	26.0
3.093	7.7	2.854	9.4	3.026	25.9
3.097	7.8	2.858	9.2	3.030	25.8
3.101	7.7	2.861	9.2	3.034	25.7
3.105	7.7	2.865	9.3	3.037	25.9
3.109	7.7	2.869	9.2	3.041	25.9
3.113	7.6	2.872	9.0	3.045	26.1
3.117	7.6	2.876	9.2	3.049	26.1
3.121	7.5	2.879	9.3	3.052	26.1
3.124	7.1	2.883	9.3	3.056	26.2
3.128	7.0	2.886	9.3	3.060	26.3
3.132	7.0	2.890	9.3	3.064	26.4
3.136	6.9	2.893	9.3	3.068	26.5
3.140	6.8	2.897	9.4	3.071	26.5
3.144	6.7	2.901	9.5	3.075	26.5
3.148	6.6	2.904	9.6	3.079	26.6

3.151	6.7	2.908	9.6	3.083	26.7
3.155	6.8	2.911	9.6	3.087	26.7
3.159	6.8	2.915	9.5	3.090	26.9
3.163	5.9	2.918	9.5	3.094	27.2
3.167	6.9	2.922	9.6	3.098	27.4
3.171	6.7	2.926	9.6	3.102	27.6
3.175	6.8	2.929	9.6	3.105	27.6
3.179	6.9	2.933	9.5	3.109	27.7
3.182	7.0	2.936	9.5	3.113	27.7
3.186	7.0	2.940	9.4	3.117	27.6
3.190	6.2	2.943	9.4	3.121	26.5
3.194	7.0	2.947	9.4	3.124	26.6
3.198	6.9	2.951	9.5	3.128	26.4
3.202	7.0	2.954	9.5	3.132	26.3
3.206	7.0	2.958	9.6	3.136	26.2
3.209	7.1	2.961	9.5	3.139	26.0
3.213	7.1	2.965	9.7	3.143	25.9
3.217	7.1	2.968	11.1	3.147	25.7
3.221	7.0	2.972	11.1	3.151	25.7
3.225	7.1	2.976	9.9	3.155	25.7
3.229	7.2	2.979	9.9	3.158	25.8
3.233	7.3	2.983	11.2	3.162	25.8
3.237	7.4	2.986	11.4	3.166	25.8
3.240	7.4	2.990	11.5	3.170	25.9
3.244	7.5	2.993	11.5	3.174	26.0
3.248	7.5	2.997	11.5	3.177	26.2
3.252	7.5	3.001	11.6	3.181	26.2
3.256	7.5	3.004	11.6	3.185	26.5
3.260	7.6	3.008	11.6	3.189	26.7
3.264	7.5	3.011	11.5	3.192	26.9
3.267	7.6	3.015	11.5	3.196	27.2
3.271	7.7	3.018	11.5	3.200	27.6
3.275	7.8	3.022	11.5		
3.279	8.0	3.025	11.5		
3.283	8.1	3.029	11.7		
3.287	8.3	3.033	11.7		
3.291	8.3	3.036	11.8		
3.295	8.5	3.040	12.1		
3.298	8.7	3.043	12.2		
3.302	8.8	3.047	12.2		
3.306	8.8	3.050	12.1		

3.310	8.9	3.054	12.3		
3.314	8.9	3.058	12.4		
3.318	9.1	3.061	12.7		
3.322	9.1	3.065	12.8		
3.325	9.2	3.068	12.9		
3.329	8.5	3.072	13.0		
3.333	8.5	3.075	13.0		
3.337	8.6	3.079	13.1		
3.341	8.7	3.083	13.2		
3.345	8.8	3.086	13.1		
3.349	8.9	3.090	13.0		
3.353	8.9	3.093	12.8		
3.356	9.0	3.097	12.6		
3.360	9.2	3.100	12.5		
3.364	9.2	3.104	12.3		
3.368	9.3	3.108	12.2		
3.372	9.4	3.111	12.0		
3.376	9.5	3.115	11.9		
3.380	9.6	3.118	11.7		
3.383	9.7	3.122	11.5		
3.387	9.8	3.125	11.3		
3.391	9.8	3.129	11.1		
3.395	9.9	3.133	11.0		
3.399	10.0	3.136	10.8		
3.403	10.1	3.140	10.6		
3.407	10.3	3.143	9.5		
3.411	10.4	3.147	9.4		
3.414	10.6	3.150	9.3		
3.418	10.6	3.154	10.2		
3.422	10.7	3.157	10.1		
3.426	10.7	3.161	10.0		
3.430	10.6	3.165	9.9		
3.434	10.6	3.168	9.8		
3.438	10.5	3.172	8.6		
3.441	10.4	3.175	9.7		
3.445	10.4	3.179	9.6		
3.449	10.3	3.182	9.5		
3.453	10.2	3.186	9.4		
3.457	10.2	3.190	9.4		
3.461	10.1	3.193	9.4		
3.465	10.1	3.197	9.5		

3.469	10.0	3.200	9.5		
3.472	10.0	3.204	9.5		
3.476	9.9	3.207	9.5		
3.480	9.7	3.211	9.6		
3.484	9.6	3.215	9.6		
3.488	9.6	3.218	9.9		
3.492	9.6	3.222	9.9		
3.496	9.5	3.225	9.8		
3.499	9.4	3.229	9.7		
3.503	9.2	3.232	8.7		
3.507	9.1	3.236	8.7		
3.511	9.0	3.240	8.6		
3.515	9.0	3.243	8.6		
3.519	9.0	3.247	8.6		
3.523	9.1	3.250	8.4		
3.527	9.3	3.254	9.5		
3.530	9.4	3.257	8.4		
3.534	9.5	3.261	8.4		
3.538	9.7	3.265	9.5		
3.542	9.7	3.268	9.5		
3.546	9.9	3.272	8.5		
3.550	9.8	3.275	8.6		
3.554	9.8	3.279	8.7		
3.557	9.8	3.282	8.7		
3.561	9.9	3.286	8.7		
3.565	9.8	3.290	8.8		
3.569	9.9	3.293	8.9		
3.573	10.0	3.297	9.0		
3.577	10.0	3.300	9.2		
3.581	10.2	3.304	9.2		
3.585	10.2	3.307	9.3		
3.588	10.4	3.311	9.4		
3.592	10.6	3.314	9.5		
3.596	10.7	3.318	9.7		
		3.322	9.8		
		3.325	9.9		
		3.329	9.9		
		3.332	10.0		
		3.336	10.3		
		3.339	10.4		
		3.343	10.4		

A-23

		3.347	10.5		
		3.350	10.7		
		3.354	10.1		
		3.357	10.3		
		3.361	10.5		
		3.364	10.6		
		3.368	10.9		
		3.372	11.3		
		3.375	11.6		
		3.379	11.9		
		3.382	12.2		
		3.386	12.5		
		3.389	12.7		
		3.393	13.0		
		3.397	13.2		
		3.400	13.5		
		3.404	13.8		
		3.407	14.1		
		3.411	14.4		
		3.414	14.7		
		3.418	15.1		
		3.422	15.5		
		3.425	15.8		
		3.429	16.3		
		3.432	16.7		
		3.436	17.1		
		3.439	17.4		
		3.443	17.8		
		3.446	18.2		
		3.450	18.5		
		3.454	18.8		
		3.457	19.1		
		3.461	19.4		
		3.464	19.7		
		3.468	20.0		
		3.471	20.3		
		3.475	20.9		
		3.479	21.5		
		3.482	22.3		
		3.486	22.9		
		3.489	23.4		

		3.493	24.1		
		3.496	24.8		